



This is to certify that the

thesis entitled

Comparison of the cooling effectiveness of superheated steam and hotain in internal furbine blade cooling

Ramakrishnan Pudupatty

has been accepted towards fulfillment of the requirements for

Masters (M. Spegree in Mechanical Engineering

Date 4/27/98

Major professor

O-7639

MSU is an Affirmative Action/Equal Opportunity Institution



PLACE IN RETURN BOX to remove this checkout from your record. TO AVOID FINES return on or before date due.

DATE DUE	DATE DUE	DATE DUE

1/98 c/CIRC/DateDue.p65-p.14

COMPARISON OF THE COOLING EFFECTIVENESS OF SUPERHEATED STEAM AND HOT AIR IN INTERNAL TURBINE BLADE COOLING

By

Ramakrishnan Pudupatty

A THESIS

Submitted to
Michigan State University
in partial fulfillment of the requirements
for the degree of

MASTER OF SCIENCE

Department of Mechanical Engineering

1998

ABSTRACT

COMPARISON OF THE COOLING EFFECTIVENESS OF SUPERHEATED STEAM AND HOT AIR IN INTERNAL TURBINE BLADE COOLING

By

Ramakrishnan Pudupatty

Turbine inlet temperatures continue to increase, and this increase in temperature has led to an unfavorable combination of thermal stresses, oxidation and creep in the hot sections of the turbine engine components, particularly in the turbine blades section. The reduction of the blade temperature to an appropriate level in order to maintain the material integrity and decomposition of temperature gradients in the blade profile sections becomes a principal concern. Combination of various cooling methods and cooling agents are used to address this problem and the current discussion concentrates on comparing the heat transfer characteristics of compressed air and super heated steam in a single pass internal cooling configuration, both experimentally and numerically. The experiments establish a base line data for the internal coolant capabilities of steam and air on the basis of heating tests on a simple flat blade geometry. Once the base line data have been established, the coolant properties of air and steam are compared and an evaluation of the experimental technique for conduction and convective heat transfer for this geometry is performed using analytical tools to compare the experimental results with the analytical predictions. The experimental surface temperatures are measured using precisely calibrated liquid crystals, and the temperature gradients above the blade are determined using specially designed thermocouple probe and the numerical validation is done using ANSYS53 package.

ACKNOWLEDGEMENTS

I would like to express my gratitude for the thoughtful and patient guidance of my advisor, Dr. John R. Lloyd, throughout my graduate program. The assistance of my master's committee members, Dr. Mei Zhuang and especially Dr. Abraham Engeda, for his patience and confidence in me, are gratefully acknowledged. Their insightful comments were particularly helpful in placing my work in perspective.

Special thanks are due to Roy Bailiff, for his extensive assistance in building the test rig. Thanks are due to Gloria Elliott, Ramez Abdulnour and Paul Hoke for their thoughtful comments. Thanks are also given to my dear friends who have listened and offered support.

This research was funded by the U.S. Department of Energy.

Finally, a special thank you to my parents, brother and sisters, for their patience, encouragement and confidence.

TABLE OF CONTENTS

LIST OF FIGURES	v
NOMENCLATURE	vii
INTRODUCTION	1
LITERATURE REVIEW	10
EXPERIMENTAL APPARATUS	21
RESULTS AND DISCUSSION	30
CONCLUSIONS	47
APPENDICES	48
REFERENCES	92

LIST OF FIGURES

Figure 1. Illustration of various cooling modes	3
Figure 2. Schematic of Internal Turbine blade cooling in a	
modern turbine blade cross section	7
Figure 3. Photograph of the Experimental Setup	
Figure 4. Experimental Setup for the Hot air configuration	
Figure 5. Experimental Setup for Super Heated Steam Configuration	
Figure 6. Schematic of the One pass test blade	
Figure 7. Calibration Facility of Liquid Crystals	
Figure 8. Typical HSI signals used for calibration of Liquid Crystals	
Figure 9. Polynomial fit for the calibration data of Liquid crystals	
Figure 10. Corrected Configuration of the blade	
Figure 11. A typical velocity profile on the electrically heated flat blade	
(At the location $x/L = 0.72$ from the leading edge)	35
Figure 12. A typical temperature profile over the electrically heated blade	
surface (At the location x/L= 0.72 from the leading edge)	36
Figure 13. Local Nusselt Number versus Local Reynolds Number for	
an Electrically heated plate	36
Figure 14. Illustration of the electrical analogy model set up to compute 'hin'	37
Figure 15. Dimensionless Temperature Profile at 4.194cm from the leading	
edge with hot air being circulated internally	39
Figure 16. Dimensionless Temperature Profile at 4.194cm from the leading	
edge with super heated steam being circulated internally	39
Figure 17. Average Internal Nusselt Number versus Average Internal	
Reynolds Number	40
Figure 18. Local Nusselt Number versus dimensional distance in the	
direction of internal flow	41
Figure 19. ANSYS 3D Numerical Model that was built to verify	
the experimental assumptions	42
Figure 20. Computed velocity profile of the internal fluid at the center	
cross section in the external flow direction	44
Figure 21. Temperature Profile of the internal fluid across the middle	
along the external flow direction	
Figure 22. Temperature Profile of the internal fluid from inlet to exit	46
Figure A1. Velocity profile of the air flow across the width of the	
test section for an entrance length of 0.9m	50
Figure A2. Velocity profile of the air flow across the width of the	
test section for an entrance length of 1.2m	50
Figure A3. Velocity profile of the air flow across the width of the	
test section for an entrance length of 2.1m	51
Figure A4. Velocity profile of the air flow from top to bottom of the	

test section for an entrance length of 0.9m	52
Figure A5. Velocity profile of the air from top to bottom of the	
test section for an entrance length of 1.2m	52
Figure A6. Velocity profile of the air flow from top to bottom of	
the test section for an entrance length of 2.1m	53
Figure B1. Calibration Facility of Liquid Crystals	64
Figure B2. Comparison of 8 bit versus 24 bit values	66
Figure C1. Overall System Design	70
Figure C2. Flowchart of the control algorithm	
Figure C3. Second Order Polynomial Fit for Hue versus Temperature	75

NOMENCLATURE

 T_{g} Temperature of the hot gas, K T_{c} Temperature of the coolant fluid, K V_{g} Velocity of the hot gas, m/s V_c Velocity of the coolant fluid, m/s **RGB** Red, Green and Blue HSI Hue, Saturation and Intensity distance along the external flow direction from the leading edge of the X blade, m distance normal to the flat blade surface, m y distance along the internal flow direction, m Z L total length of the blade from the leading edge along the external flow direction, m Y total internal flow opening in the blade in the 'y' direction, m Z total length of the blade along the internal flow direction, m D_h hydraulic diameter, m external convective heat transfer coefficient (of air), W/m²K hext internal convective heat transfer coefficient (of hot air, super heated hin steam), W/m²K thermal conductivity of air close to the wall, W/mK k_{ext} (dT/dy)_{ext} temperature gradient of the external flow(air) in a direction normal to the flow, near the wall, K/m

 $Nu_x(or)Nu_{x,ext}$ local external nusselt number, based on the local distance from the leading edge of the blade

Nu, Nu_{Dh} internal Nusselt number based on the hydraulic diameter

 $Re_x(or)Re_{x,ext}$ local external reynolds number, based on the local distance from the leading edge of the blade

Re, Re_{Dh} internal reynolds number based on the hydraulic diameter

Pr prandtl Number of gas

T_{amb.} T_{ext} external flow (air) temperature, K

T_{w.} T_{s.ext} external surface (copper) temperature, K

T_{in} internal flow (hot air or super heated steam) temperature, K

t thickness of the copper surface, m

 k_{cu} thermal conductivity of copper, W/mK

A_{cu} cross sectional area of the copper surface, m²

A_{ext}, A_{in} cross sectional area in the direction of heat transfer, m²

INTRODUCTION

In the development of aircraft and land based power plants serious difficulties are encountered in the effort to cool certain structural elements - combustion chamber walls, nozzles, or gas turbine blades - against the influence of the hot gases. The maximum cycle temperature at which gas turbines are designed to operate is increasing as rapidly as the technology of high temperature materials and cooling methods will allow. All modern aircraft as well as industrial power producing gas turbines, operate at cycle temperatures which require turbine vane and blade cooling, as well as special cooling configurations for other hot section components such as combustors etc. In conjunction with blade cooling, special considerations in materials and coating selections are required to insure the reliable operation of these advanced engines. New cooling methods have been proposed and are being developed to meet this requirement.

High gas temperatures of 1600 to 1800 K require sophisticated cooling mechanisms. The cooling has the same functions for both the rotor as well as the stator blade namely:

- (1) reduction of the blade temperature to a level which is appropriate to maintain material integrity, and
- (2) decomposition of temperature gradients in the blade profile sections, to avoid steep temperature gradients and thus avoid thermal stress.

Turbine inlet temperatures continue to increase, but the rate of increase is slowing down because most of the malfunctions that occur during the operation of these engines

originate in its hot sections, thereby reducing the overall efficiency. The reduction of fuel consumption, which is necessary for improving the overall cooling efficiency of turbine blades, can be achieved not only by improving the component efficiencies but by also increasing the turbine inlet temperature and the pressure ratio. These improvements require active cooling of the hot turbine components in order to avoid a reduction of operating life due to an unfavorable combination of oxidation, creep, and thermal stresses. However, the coolant mass flow rate can become so large that the excess compressor (in the gas turbine power cycle) power for cooling can offset the power gains associated with an incremental increase in turbine inlet conditions. Low grade fuels introduce corrosive agents into the hot stream and the metal temperature of hot components may have to be reduced to avoid corrosion. This reduction in metal temperatures results in increased demand of cooling drawn from the compressor and, hence in performance penalty. In order to optimize the above factors there is a need to not only improve the existing cooling configurations but also to look for new alternative cooling agents.

Prior to a detailed study about the heat transfer aspects of the coolants, in particular steam, a brief introduction about the various modes of the cooling methods that are currently being used in the hot sections of turbine blades is discussed. Figure 1 shows a sketch of the different blade cooling configurations. Figure 1(a) shows the standard internal convection cooling method. Figure 1(b) is the film cooling process in which a stream of coolant is blown through a series of slots in a direction that is inclined at an angle to the surface. In this way a layer which insulates the wall from the hot gases is

created. The coolant film is gradually destroyed by mixing with the hot gases so that its effectiveness decreases in the downstream direction. This disadvantage can be avoided by the process indicated in figure 1(c) called transpiration cooling. In this method the wall is manufactured from a porous material and the coolant is blown through the pores. The coolant film on the hot gas side is, therefore, continuously renewed and the cooling effectiveness can be made to stay constant along the surface. A principal disadvantage of this mode of cooling is the low strength of the blades.

When the hot medium is hot gas, the cooling effectiveness obtained in both transpiration and film cooling can be substantially increased by using a liquid as a coolant. In this case, which corresponds to Figure 1(d), a liquid film is created on the hot gas side. The liquid is evaporated on its surface, and the energy

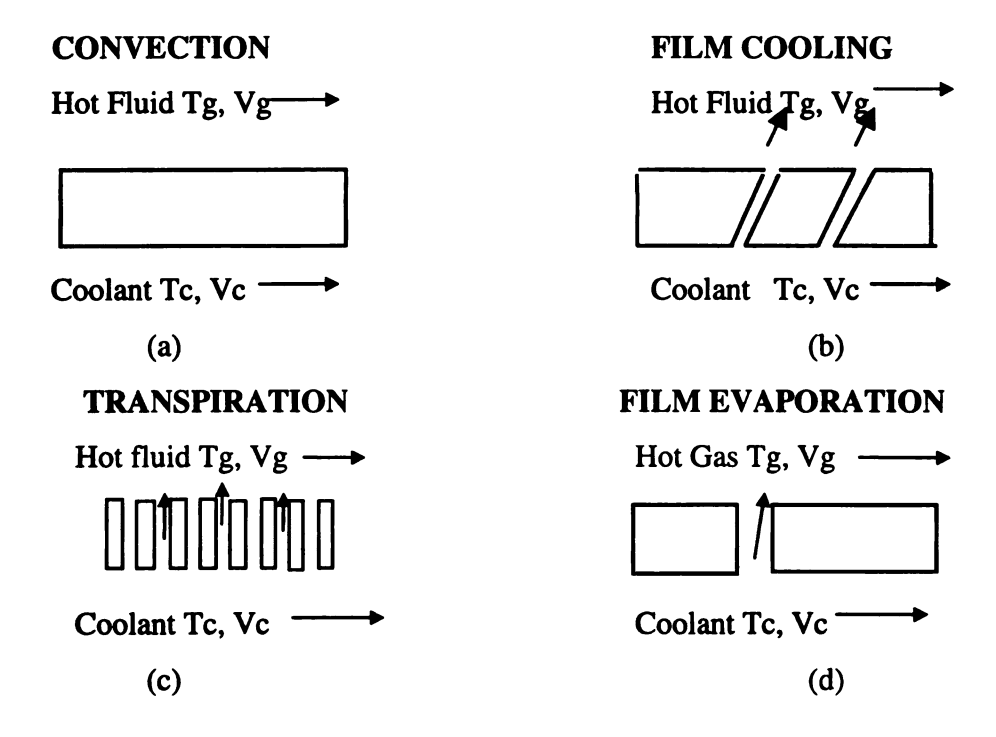


Figure 1. Illustration of various cooling modes

absorbed by the evaporation process substantially increases the effectiveness of this method. This method is known as evaporative film cooling or evaporative transpiration cooling, depending on whether the coolant is discharged through slots or through a porous wall. This method is seldom used in cooling turbine blades, and hence is not discussed in detail in this report.

Air is a good cooling medium for the processes mentioned above because of the fact it can be continuously provided at places where engines are used. At higher speeds the temperature of the air increases, and so it is often useless as a coolant unless its temperature is decreased by some cooling cycle. The cooling process consumes power and weight and necessitates reducing the amount of coolant air required to a minimum. In this respect a coolant with a better heat carrying capacity can be used as a substitute for air. This is the focus of current research where the cooling potential of steam which has a better heat carrying capacity than air is evaluated. Steam also has an advantage over water, in that its much lighter than water, and thus when it is used as a coolant it can avoid the excess cost incurred in carrying a heavier coolant.

To obtain a fundamental understanding of the different types of cooling methods that have just been introduced, a uniform set of operating conditions as described below is maintained while comparing the three common configurations namely internal convection cooling, film cooling and transpiration cooling. Here a hot gas stream of temperature T_g flows adjacent to the a wall. The bulk temperature of the fluid, T_g, does not change in the

flow direction. The velocity V_g in the gas flow outside the boundary layer is also assumed constant along the wall. Under normal conditions, the thickness of the boundary layer is so small such that the curvature effects due to the blade geometry do not play a significant role. Consequently for this present work a flat plate subjected to hot gas flow on either side with uniform temperature T_g and Uniform velocity V_g is considered (Figure 1). The temperature drop through the wall is assumed to be negligible compared with that of the coolant and hot gas side.

In an internal convection cooling arrangement, the cooling stream flows along the coolant side of the blade wall as shown in Figure 1(a). The coolant flow has to be limited for reasons stated earlier, and hence the coolant medium gets heated up considerably on its passage through the blade. Optimum conditions for convection cooling are obtained by increasing the surface area on the coolant side of the wall by adding fins. The strength characteristics of the wall material prescribe a certain wall temperature that can be tolerated. Optimum conditions are attained when the entire surface is kept at that temperature. Overcooling of certain sections consume more coolant. This constant wall temperature can be obtained either by varying the fin surface area along the cooling path in order to compensate for smaller temperature differences between the wall and the coolant medium, by increasing the coolant medium velocity toward the downstream end of the surface, or by a combination of both.

In the internal cooling method, the coolant from the compressor is introduced through the hub section into the blade interior, and then discharged out of the blade trailing edge.

Radially aligned coolant channels of basically rectangular cross section are used

extensively to cool the mid chord regions of turbine blades; these channels are connected by 90 and 180 degree turns to form serpentine cooling passages as shown in Figure 2. Frequently these passage surfaces are roughened with ribs to enhance the convective heat transfer. It is well known that both the nature of the flow and the associated convection heat transfer are usually significantly altered in and around the turn. In general, the centrifugal forces present in a turning flow induce secondary flows which have the effect of augmenting heat transfer in the streamwise direction.

Film cooling, shown in Figure 1(b), is comprised of introducing a secondary fluid, at one or more discrete locations along the airfoil surfaces or endwalls, which are exposed to a high temperature environment. The objective is to protect the surfaces, not only in the immediate region of the injection sites, but also in the downstream region. The introduction of cooler fluid into the boundary layer produces an insulating layer between the wall to be protected and the gas stream flowing over it. Additionally, the injected fluid mixes with the mainstream can be considered as a heat sink, that effectively lowers the mean temperature in the boundary layer. Another benefit of film cooling is that it not only protects the surface downstream of injection, but it also provides convective heat transfer cooling on the surfaces of the film injection holes. Usually spent coolant from internal cooling can be further used for film cooling.

The coolant is ejected through slots in a direction parallel to the surface. A cool film is built up, but it is gradually destroyed by turbulent mixing and heat conduction from the

hot gas flow. The cooling film can be renewed by arrangements of addition slots arranged at certain distances downstream. No uniform wall temperature is possible for film cooling.

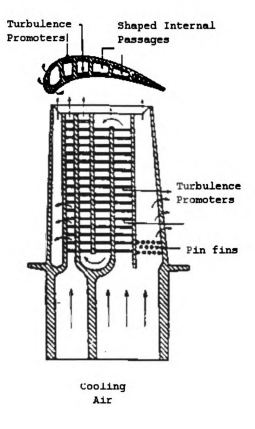


Figure 2. Schematic of Internal Turbine blade cooling in a modern turbine blade cross section (Han J.C.(1986))

The wall is coolest near a slot and increases in temperature downstream of the slot hole. The temperature of the wall which would eventually attain the gas temperature at sufficient distance from the slot can be decreased by increasing the number of slots.

The arrangement for transpiration cooling is shown in Figure 1(c). For this cooling method, the wall is fabricated from porous material, and the coolant medium passes through the wall in the gas flow. A protective film builds up on the gas side of the wall and insulates it from the hot gas stream. The cooling air is directed away from the surface as it leaves the wall. In this way, a counterflow condition is created between the heat carried away from the surface with the coolant stream and heat transferred from the hot gas toward the wall. This counterflow reduces the overall heat transfer between the gas and the wall surface. Another advantage of this cooling method is based on the fact that the area of contact between the coolant medium on its way through the wall and the wall material is very large. As a consequence the coolant medium will be heated up almost to the wall temperature. A constant wall temperature can be obtained over the entire surface by proper adjustment of the local coolant flow through the porous wall.

The comparison of the different modes of cooling can be made with respect to the highest wall temperature. This basis somewhat underestimates film cooling because the average wall temperature for this method is lower than that for the previously described transpiration and convection cooling method, when the maximum temperatures are adjusted equal for all three methods. Therefore, parts of film cooled wall will have lower temperatures and better strength, and to a certain extent, these parts can support the hot

portions of the wall. Consequently, under the same strength limitations, the maximum temperature of the film cooled wall could be somewhat higher than the temperatures for comparable transpiration and convection cooled walls. But convection cooling normally requires more coolant flow compared to the other two modes of cooling, while the strength of blades becomes relatively low when transpiration cooling is used extensively. Considering the above advantages and disadvantages, the combination of internal cooling with film cooling becomes a highly attractive scheme, and this is what is being currently used in cooling turbine blades.

LITERATURE SURVEY

Chyu (1991) has actively investigated turning flow and heat transfer in different channel cross-sectional geometry's. These studies investigated the turning induced secondary flow fields and their effects on heat transfer and head loss. Metzger et.al (1968, 1973, 1985) have published a series of studies on flow visualizations, pressure measurements, and heat transfer characteristics for a large family of smooth and rough channels. Boyle (1984) reported the distribution of heat transfer coefficient along the centerline of channel span for both smooth and rough surfaces. Murthy and Chyu (1987) numerically modelled the laminar flow and heat transfer with passage rotation. Wagner et.al (1986) experimentally investigated the rotational effects on regional heat transfer. Chyu (1991) investigated the regional heat transfer in two and three pass passages with 180 degree sharp turns. Russell et. al (1993) generated a set of experimental data in order to validate the computer codes that existed for internal cooling systems and found major inconsistencies suggesting the need for further computational studies on complicated geometry's. Zhang et.al (1991) performed experiments to determine the local heat transfer performance in a rotating serpentine passage with rib roughened surfaces. They found that the there was a significant heat transfer enhancement in both stationary and rotating cases resulting from an installation of the ribs.

Recent activity in internal flow heat transfer related to blade cooling has been centered around rotation effects, impingement cooling and pin fins. Abe et. al (1984) describe

turbine blade cooling which incorporates convection cooling with different pin fins in the mid chord and trailing edge regions, impingement cooling on the inside of the leading edge, and film cooling on the leading edge (showerhead) and pressure surface.

Mori et. al (1971) reported effects of rotation on heat transfer from a rotating circular tube, and Johnson et.al showed that the effect of rotation was to change the effect of turbulence near the leading and trailing walls of a rectangular passage in a fully developed flow. Wang's (1993, 1994) studies of impingement cooling have been concerned with the effects of crossflow of spent fluid and the geometry of the jet array, and the influence of heat transfer around holes in the target plate. Hollworth et.al (1983) conducted a detailed study of heat transfer to a target plate equipped with vent holes. The authors concluded that the high performance came, not from the increased heat transfer around the vent holes, but because of reduced entrainment of heated air into the impinging jets.

Convection cooling in almost capillary passages is used in several structures. In general, these are laminated, diffusion bonded, multilayer assemblies with high heat transfer area per unit volume inside a sheet of material which appears to be perforated. This laminated structure is used as a non load bearing aerodynamic shell attached to a load bearing spar, which is well protected from the gas stream. Effusion of the coolant through the holes can be described either as transpiration or as diffusion hole injection, depending on the spacing and size of the holes and on the ejection velocity.

One of the earliest works in transpiration cooling was done by Eckert and Livinghood (1954). Transpiration cooling is one of the most effective methods for protecting a surface exposed to a hot gas stream. The coolant penetrates into the bottom of a porous plate and exchanges heat with the porous medium, and blows off from the other surface of the test porous plate. Kikkawa et. al.,(1991) found that because of a high heat exchange between the coolant and the porous medium, one can expect a much higher cooling effectiveness by transpiration than by film cooling, in spite of a low consumption of coolant.

There have been many experiments on heat transfer with transpiration, beginning in the early 1960s and covering many situations. The earliest studies done by Torii (1966) were on smooth, flat plates with uniform transpiration and uniform free stream velocity. Similar studies were performed by Moffat et.al (1966). Next came studies of accelerating flows and decelerating flows which were done by Thielbhar (1970, 1972). Rough surfaces with transpiration were covered by Healzer and Pimeta (1978) and rough walls with transpiration and acceleration by Coleman (1977). Moffat (1987) reports that most investigators have not focussed on the cooling effectiveness, but only on the decrease of the heat transfer coefficient with gas injection. In particular, very few papers have been published on the investigations of transpiration cooling. In Kikkawa's (1991) work on transpiration cooling, the experimental results were compared with a one dimensional theoretical analysis.

Due to limitations for developing heat transfer coefficients associated with internal cooling and the amount of coolant consumption, internal convective cooling alone cannot meet the cooling requirements at turbine inlet temperature above a certain value. Film cooling is a means for meeting more difficult cooling requirements and provision of better cooling effectiveness.

There has been considerable research over the past 30 years to increase our understanding of coolant film behavior and its interaction with free stream flow. The film cooling literature is extensive, and references [Goldstein(1971), Metzger(1968,1973), Sasaki(1979), Ito(1978), Dring(1980)] provide a reasonable sampling of many of the early works. Many of these earlier works looked at only the adiabatic effectiveness and the factors which affected it. They rely on the assumption that the heat transfer coefficient could be taken from data. With the prospect of full coverage film cooling it became necessary to document both the heat transfer and the effectiveness to have a complete description of the situation.

Kasagi et.al(1981) and Kumada et. Al. (1981) looked at both the film cooling effectiveness and the heat transfer properties on a film cooled surface and also the heat transfer properties of the impingement cooled back face of that surface. The combination of impingement with film cooling employing the spent coolant has been used in several designs.

Work on film cooling has examined the interaction of curvature with other effects and the structure of turbulence in the full coverage, film cooled boundary layer on a convex wall, as done by Hay(1985). Goldstein et. al (1971) showed that surface roughness affects the average effectiveness for single and double rows of holes. They also showed that the secondary flows can strip the coolant away from the suction surface of a vane over a significantly large region near the hub

Remarkably little has reached the open literature about the losses incurred with film cooling. Favorskii and Kopelov(1981) estimated that each 1% of cooling air discharged through the blades dropped turbine efficiency by 1%. They also documented the increased vibration resulting from leading edge injection. Louis(1981) pointed out that profile losses for film cooling are linearly proportional to the thickness of the injected flow, though the effectiveness is not. Kawaike et.al.(1994) concluded that there are significant performance advantages to be gained by passing cooling air completely through the vanes, thence to an intercooler, and using the same air to cool the associated rotor blades. This treatment avoids more than half the thermodynamic penalty associated with the mixing of low temperature coolant with the mainstream.

Dunn and Hause (1981), reported an increase in stator vane heat transfer associated with the presence of an active rotor, and cautioned against the use of stator only data to characterize full stage behavior. Dring (1982) measured the heat transfer on rotor blades and stator vanes. Further evidence of the influence of the rotor on heat transfer to the

stator was reported by Dunn(1984). Hay et.al (1985) investigated the effects of cooling films on the heat transfer coefficient on a flat plate with zero mainstream pressure gradient, by injecting the coolant at different angles. They found that the heat transfer coefficient values increased near the injection holes, but still called for basing realistic design of film cooled components on heat transfer coefficient with injection. Ekkad et.al (1995) investigated the effect of the coolant blowing ratio on the film cooling performance. Hempel et.al (1980) investigated the performance of full coverage film cooled blades and found that under certain specific conditions full coverage film cooling approaches the cooling effectiveness of transpiration cooling. Shen et.al (1994) investigated the heat transfer enhancement within a turbine blade cooling passage using ribs and combinations of ribs with film cooling holes. Gillespie et.al (1994) did some local heat transfer measurements in the entrance to normal and inclined film cooling holes.

Improvements in air cooling techniques are actively being pursued for aircraft engines, but other cooling technologies using water and superheated steam are being considered for ground based power plants. Although air will always be the primary choice as the coolant for aero engines, there very likely will be situations where the use of other fluids like water and superheated steam will be appropriate. Eckert (1954) was farsighted enough to understand this 40 years ago, and the application of this method of cooling to stationary gas turbines is now being studied.

Rice(1980) proposed steam as a cooling agent for cooling gas turbine blades and vanes in a combined cycle for ground based power generation. Also, cooling of the air by some means such as water injection or compact low weight heat exchangers may become attractive. Louis and Wu (1984) have studied this aspect of the problem and have concluded that the enhancement performance of combined cycles using steam cooled gas turbines, particularly film steam cooling, is very favorable. The advantages of this technique derives from the high specific heat of steam, negligible pumping power, but most significantly from the fact that the steam is developed using the waste heat from the gas turbine and then expands through the gas turbine with the combustion gases. Rice(1982), in his work on the reheat gas turbine with steam blade cooling, stated that the reheat pressure and hence the reheat temperature can be appreciably increased by applying steam cooling to the gas generator turbine blades. It has been found by Rice that as the reheat pressure level is increased, the performance of the gas turbine cycle is increased, and at the same time the physical size of the reheat combustor is reduced, thereby enhancing its practicality.

Aircraft technology can be successfully implemented for industrial applications. Studies have shown that steam extracted from the associated steam turbine cycle in a combined cycle can be substituted for air as the blade coolant to achieve an inlet turbine temperature of 2400°F. Wu and Louis (1984) have found that superheated steam could be introduced with minimum design changes in air cooled gas turbine technology. They

proved that the efficiency of a steam cooled combined cycle optimized at higher values of turbine inlet temperature, gas turbine pressure ratio and steam inlet pressure than the comparable cycles using air as a coolant.

Arseniev et.al(1991) in their work on combined cycle plant based on high temperature steam cooled gas turbine have indicated that it would be advantageous to employ steam for gas turbine cooling systems. They extracted the steam for the cooling system from the steam turbines and returned it back for superheating purposes. Their work confirmed the practical realization of combined plant cycle while providing higher turbine output cycle efficiencies.

Film cooling has been used for protecting turbine blades and vanes from the surrounding high temperature gas stream. In aircraft turbine applications, the majority of the studies have used air as the cooling fluid. A theoretical study by Han et.al (1986) predicted that film cooling effectiveness of steam is about twice that of air under the same operating conditions due to its favorable thermal properties such as specific heat and prandtl number. Conklin, et.al (1983) have studied film cooling effectiveness with steam injection through three staggered rows of holes that are inclined at an angle of 60 degrees over a symmetric aluminum airfoil. They found that film cooling effectiveness increased 50-150% over air cooling when steam injection was used.

Han et.al(1986) have studied the heat transfer and film cooling of a single row of inclined

holes on a stainless steel flat plate. The results showed that the film cooling effectiveness using steam was about 30 to 60 percent higher than that when air was used. The heat transfer was about 10 to 15 percent higher for all test data. They studied the film cooling effectiveness of one row and two rows of 35 degree inclined holes over a flat plate with both steam and air injection. Their experiments proved that steam injection provided about 50 to 100 percent higher film cooling effectiveness than that for air injection. They found that in the two dimensional film cooling region i.e, at lower blowing rates and/or farther downstream locations, steam injection provided 80 to 100 percent higher effectiveness because of the favorable specific heat. However, in the three dimensional film cooling regions, i.e, higher blowing rates and/or near injection hole regions, the increase in film cooling effectiveness is reduced because the advantage of higher specific heat is reduced due to mixing of the secondary fluid and the mainstream fluid.

Rice has also looked at the possibility of using steam as a coolant for compressors and combustors. He had found that while considering a continuous turbine inlet temperature of 2400°F to 2700°F for industrial gas generators, there exists a critical ducting area between the high pressure turbine blading and the low pressure turbine blading which is subjected to a much higher temperature. The main support strut passes through this ducting area to tie the inner barrel, seals, and the rear blading to the outer casing. It is not practical to use steam as a disk and casing coolant in aircraft engines due to weight restrictions. Industrial gas turbines, on the other hand, do not have these restrictions, and steam, a far superior coolant with twice the specific heat and a lower viscosity, can be

applied as a coolant, particularly when a combined cycle using a bottoming steam turbine is contemplated.

Steam can be extracted from the steam turbine, used as a coolant and readmitted into the steam turbine at a higher temperature to obtain additional steam turbine work before being condensed. A closed system is thus possible without losing steam to the atmosphere. A higher gas turbine reheat temperature can be realized through cooling the power turbine in this manner.

Ikeguchi and Kawaike (1994) have done work on the effects of a closed circuit gas turbine cooling system on combined cycle performance. In this work they have presented comparative studies taking into account the required cooling flow to cool the blade. They compared a basic conventional blade cooling system, which used an open circuit air as its coolant with two closed circuit blade cooling systems; one using as coolant the steam extracted from and returned to the bottoming cycle, and the other using air from the compressor and fed back to the combustor. The results indicate that the full closed circuit cooling system provides significant improvements in performance over conventional open circuit air cooling systems.

Steam cooling, in some respects, is simpler than air cooling. Steam is easy to pipe and has twice the specific heat which reduces the size of cooling lines. Pressure drop is not as critical as it is for air, and greater pressure differentials are available to allow more design

freedom for heat exchange surfaces. Combining these benefits of steam in a way so as to address the present problems of heat transfer and cooling gas turbine engine components would enhance the turbine cooling design process by optimizing combinations of minimum use of coolant, minimum interference with hot gas side aerodynamics, and minimum component temperature and temperature gradient levels

Thus, the overall motivation for this work is the need for incorporating the above mentioned benefits in advancing the existing cooling techniques by using superheated steam as a coolant for turbine blades in an industrial combined gas and steam turbine cycle. The discussion concentrates on comparing the heat transfer characteristics of compressed air and super heated steam in a one pass internal cooling configuration, both experimentally and numerically. The experiments are to establish base line data for the internal coolant capabilities of steam and air on the basis of heating tests on a simple flat blade geometry. Once the base line data have been established, the coolant properties of air and steam are compared and finally evaluation of existing analytical tools for conduction and convective heat transfer for this geometry is performed to compare the experimental results with the analytical predictions.

EXPERIMENTAL APPARATUS

A specially designed suction type wind tunnel shown in Figure 3, was constructed for these studies. This wind tunnel is powered by a Dayton blower run by a 3.73kW electric motor and is capable of creating air flows up to 1811 cfm. The flow rate of the air is controlled by a ball valve which is located just upstream of the blower. The flow control valve is connected to the tunnel by a 22 cm diameter tube which expands in transition from a circular cross section to the 15 cm by 20 cm rectangular cross section of the tunnel test section. The tunnel test section is about 3m long and is made up of multiple interchangeable sections made of clear plexiglass. The model blades are mounted in the flow of the stream in a section which is 0.3m long, upstream of the blade is an entrance length section which is connected to a honeycomb structure at the inlet of the tunnel for straightening the flow in the tunnel. The maximum external side Reynolds Number that can be realized in this set of experiments is about 150,000.

Figures 4 and 5 show the overall schematic of the experimental setup for the internally heated blade experimental configurations, using hot air and super heated steam, respectively.

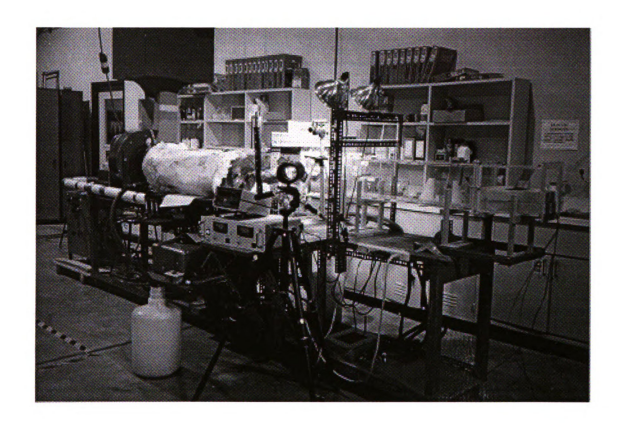


Figure 3. Photograph of the Experimental Setup

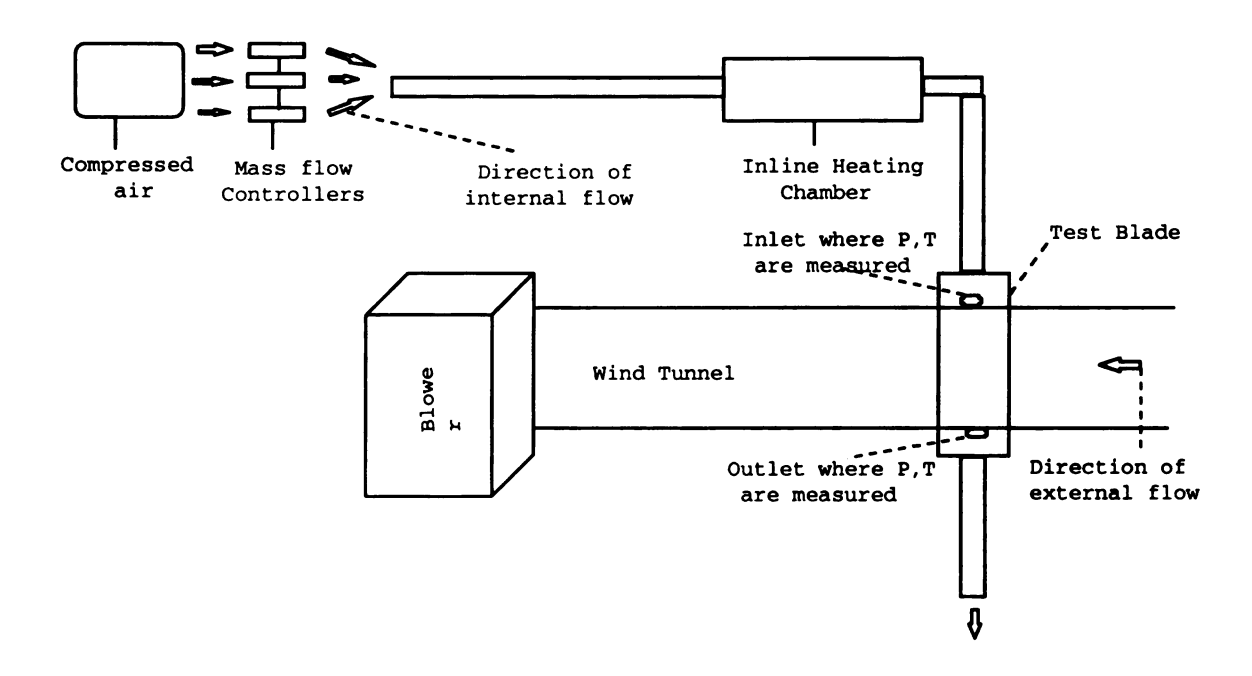


Figure 4. Experimental Setup for the Hot air configuration.

As shown in Figure 4, the compressed air from the compressor lines is passed through three Porter fast response mass flow meters and controllers (200F series). Once the required mass flow rate of air has been attained by using the built in solenoid control valve, the air is then passed through the inline heating chamber (heat exchanger) where the air is heated to the prescribed temperature. This hot air is then passed through the single pass blade, thus heating the blade internally.

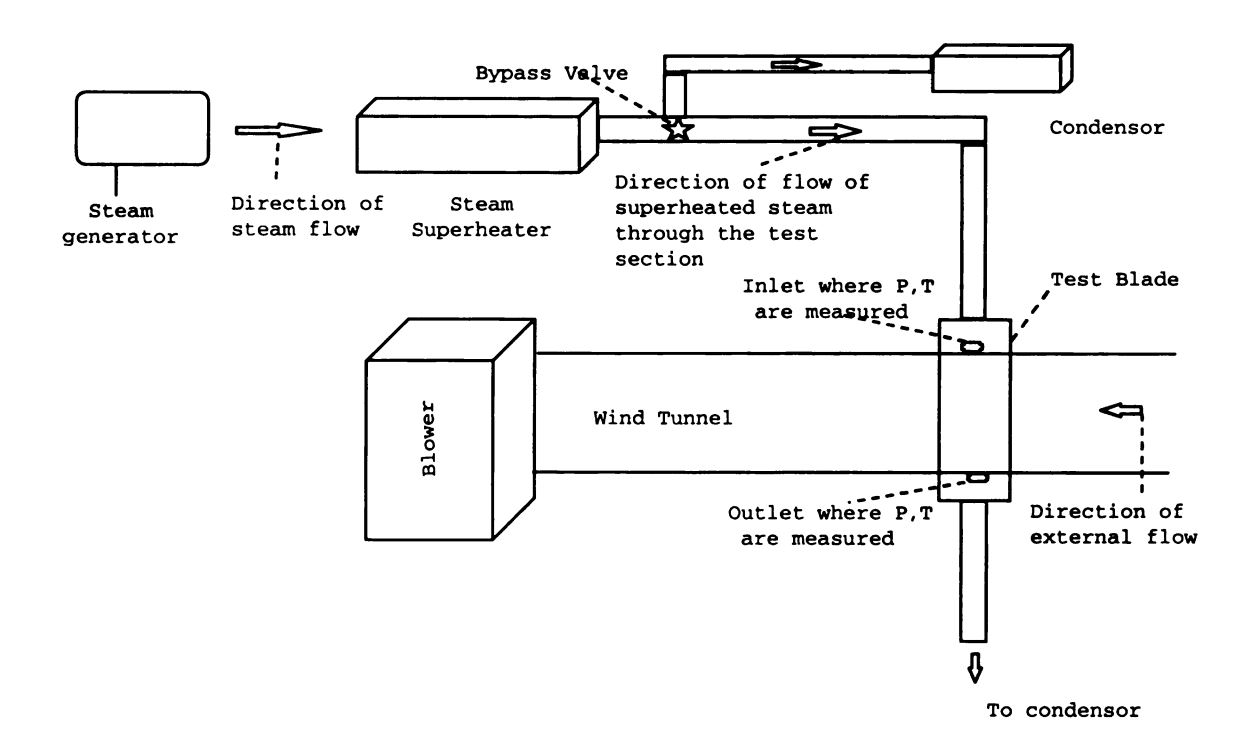


Figure 5. Experimental Setup for Super Heated Steam Configuration.

Figure 5 shows the schematic of the experimental setup for the super heated steam blade configuration. This is similar to the hot air experimental setup, with the difference being the steam generated from a Chromolax steam generator replacing the compressed air as the source. The steam, which is generated at just above saturation conditions, is then passed through a by pass valve which is used to control the mass flow rate of steam. The super heater that is present in the line is then used to superheat the steam to the prescribed state conditions, and this is then passed through the single pass blade. The steam is finally condensed in a condensor unit and the mass flow rate of the steam is measured by the condensate.

The test piece is a single pass blade made of a flattened copper tube. A cylindrical copper tube of outside diameter 169.56mm and wall thickness 1.75mm was heated and flattened to form the tube. The flattened tube consisted of three sections; a flat middle section with a cross section of 76.2mm x 6.05mm; and two curved half elliptical shaped cross sections, one at the front and the other at the back end of this rectangular cross section, with a half curvature length of 4.29mm. A sketch of the test piece used for this investigation is shown

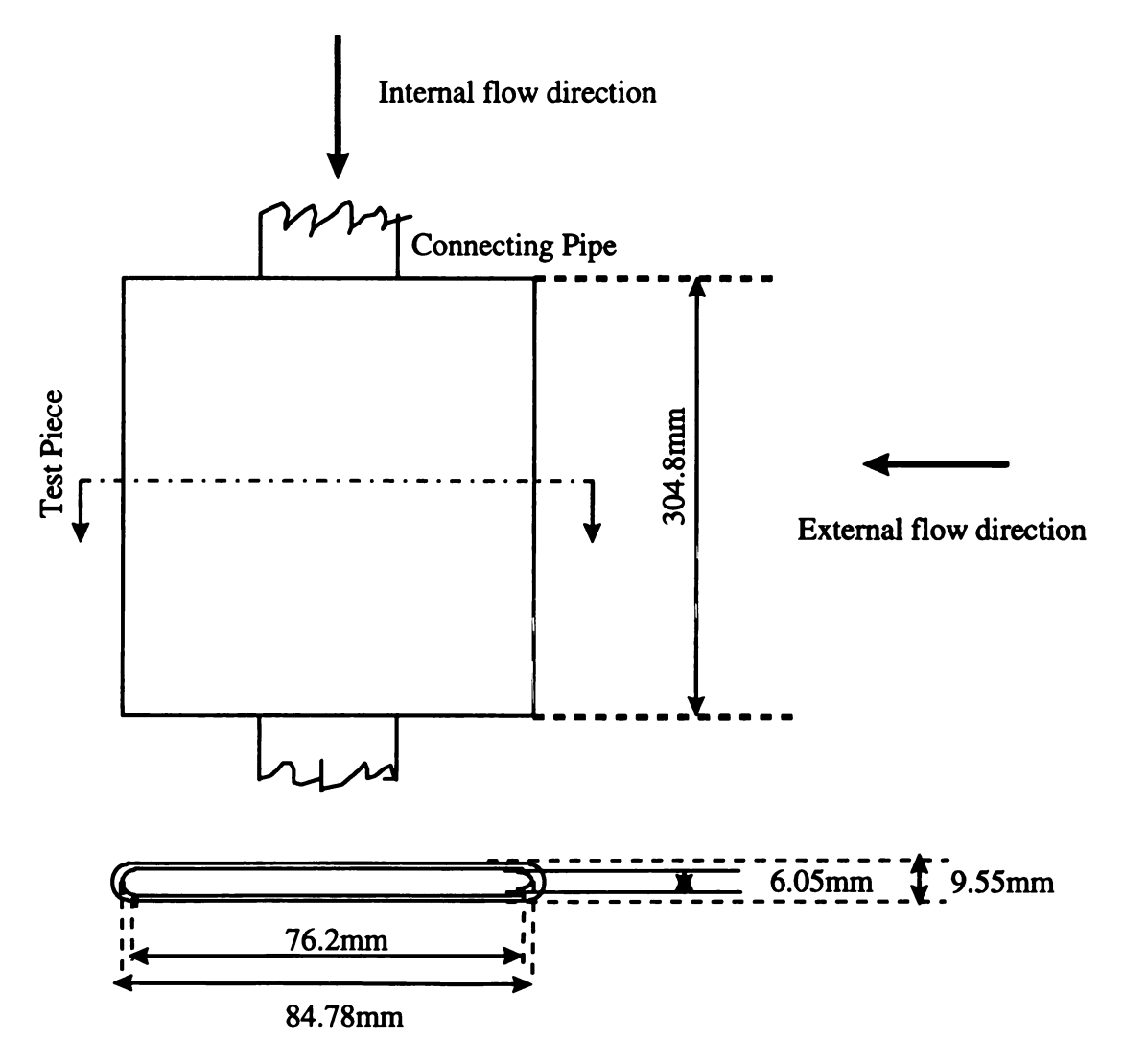


Figure 6. Schematic of the One pass test blade

in Figure 6. The entire tube is 304.8mm long. This tube is placed in the wind tunnel in such a way that the 304.8mm long section is perpendicular to the flow direction.

In order to connect this to the super heated steam and compressed air lines, a pipe fixture was mounted at the two ends of the test piece. The outer surface of the blade is coated with liquid crystals, which allows the temperature distribution on the blade surface to be determined. Before using the liquid crystals on this blade they are first calibrated in a constant temperature bath. A detailed report about the calibration procedure is attached in Appendix A and Appendix B.

Figure 7 shows the liquid crystal calibration setup. The temperature bath is fit with a PID controller unit which helps in maintaining a temperature constant to 0.1°C during the entire calibration process. To provide for the most uniform surface temperature, the liquid crystals are sprayed over a thin layer of black paint coating onto a large copper block. This block is 76.2mm square by 128.6mm high. The top is notched so that the area that the liquid crystals cover is slightly smaller than the rest of the block at only 63.5mm square. The block is placed in the constant temperature bath.

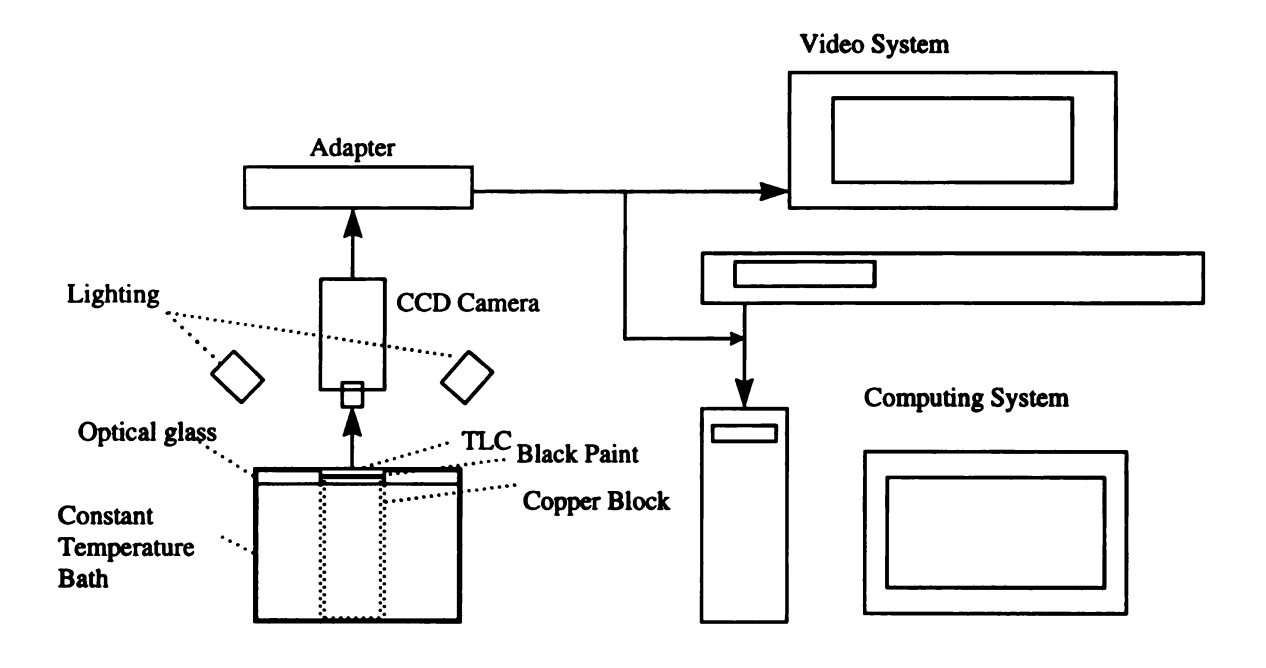


Figure 7. Calibration Facility of Liquid Crystals

This layer of liquid crystals is checked with a micrometer to ensure that they are the same thickness as the layer on the test surface. The liquid crystals used for this purpose were supplied by Hallcrest, Inc., and were of BM/R25C1W/C17-10, BM/R29C4W/C17-10, BM/R30C15W/ C17-10 and BM/R45C1W/C17-10 types. These liquid crystals showed color exhibits over a wide range off temperatures starting from 25°C to 55°C. A Sony CCD RGB camera system, including a VHS video recorder is interfaced with a 100 megahertz Pentium class computer with a Matrox Marvel image processing system using the Matlab Image Processing Tool box

The copper block is partially submerged in a constant temperature water bath which is insulated on the top by a layer of air trapped between the copper block and a flat plate of optical glass. The optical glass serves to insulate, to prevent glare, and to simulate

experimental viewing conditions. The CCD camera is set up at approximately the same angle with relation to the surface of the liquid crystals and to the lighting source as it is in the test section. A T-type thermocouple is flush mounted to one side of the copper block at a distance of 12.8mm from the top surface. This thermocouple is used to measure the temperature of the copper block during the calibration purpose. An air gap (which acts as an thermal insulating medium) is created between the coated surface and the optical glass. The illumination source is the same source used in the experimental setups.

Under steady state conditions, the optical information required to process the response of liquid crystals is recorded with the CCD RGB camera (whose position, with respect to the coated surface, was maintained constant for the calibration and for the actual experimental setup) and was either recorded on a VHS tape recorder or sent directly to the computer. A Matrox Marvel color frame grabber along with an analog processor converts the color into red green and blue components. The image data (8 bit/ 24 bit) from selected frames are processed using the software package developed for this purpose with the help of Matlab image processing toolbox to give hue, saturation and intensity content exhibited by the liquid crystals at distinct surface temperatures

After the calibration of the liquid crystals, the test piece was coated with the same type of liquid crystals. Since the test piece consisted of three different cross sections, a series of tests were initially performed on an electrically heated flat plate with a cross section similar to the one corresponding to the test piece. This was done in order to establish the measurement technique and the analysis procedure that were to be implemented, while

running tests on the internally cooled/heated test piece itself. The electrical power that was supplied to this flat blade was measured using a TEK 157 digital multimeter, which allowed both voltage and ammeter readings to be read.

These tunnel calibration experiments were carried out with an electrically heated flat plate with a curved leading edge. Its dimensions are 25.4cm long, 7.62cm wide and 0.508cm thick. The plate is capable of being operated between 0 - 600W. To measure the surface temperature of the electrically heated it was coated with a thin layer of liquid crystals. This setup enables the measurement of the whole surface temperature distribution as well as local temperature distribution in the operating temperature range of liquid crystals with the help of a frame grabber which has a capability of grabbing 30 frames/sec. With this technique of measurement, it is possible to accurately and precisely measure the surface temperature (with a temperature resolution of 0.05°C and a spatial resolution of 0.02mm) and subsequently the heat transfer on the external blade surface.

RESULTS AND DISCUSSION

The first blade that was tested was an electrically heated flat blade. The blade was first coated with a very thin layer of black background paint over which 2-3 very thin coatings (~20-30 µm thick) of liquid crystals are spray painted. The uniformity of the heat flux over the blade surface is tested by supplying and measuring the power supplied, using a TEK 157 Digital MultiMeter, to the liquid crystal coated electrically heated blade which is positioned horizontally in still air.

The calibration curves of the Hue, Saturation and Intensity values of the colors exhibited versus temperatures are shown in Figure 8. Among these three, the hue is the one that is used for this calibration because of its sensitivity and its capability to exhibit unique values at different temperatures under steady state conditions. The calibration curves compare well with those predicted by other researchers.

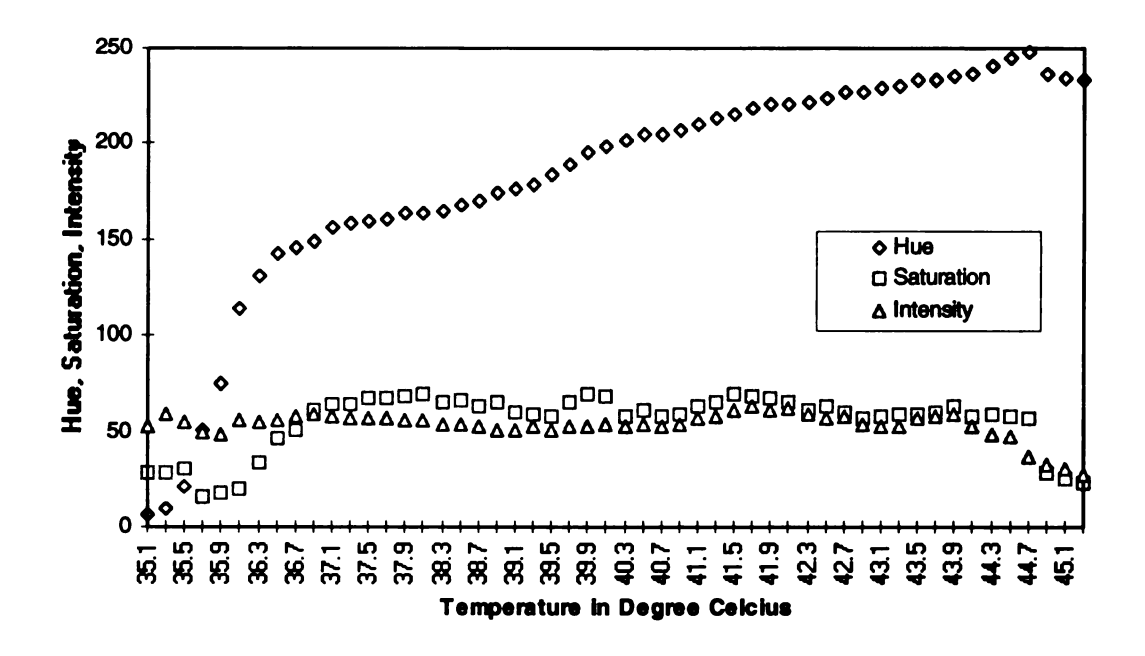


Figure 8. Typical HSI signals used for calibration of Liquid Crystals

The images were analyzed both as a 24 bit image and as an 8 bit image. It was found that under steady state conditions, these values are not very different. But because of the resolution and precise color information recorded by a 24 bit image, this was used as a standard throughout this analysis even though both the values are almost comparable.

A curve fit of second order polynomial, as shown in Figure 9, in general, agreed well with the experimental hue values. The points on this curve were within a scatter of 0.8% of the actual hue values. With this technique, it is believed that measurements can be made with a spatial resolution of 0.02mm and a temperature resolution of 0.01°C.

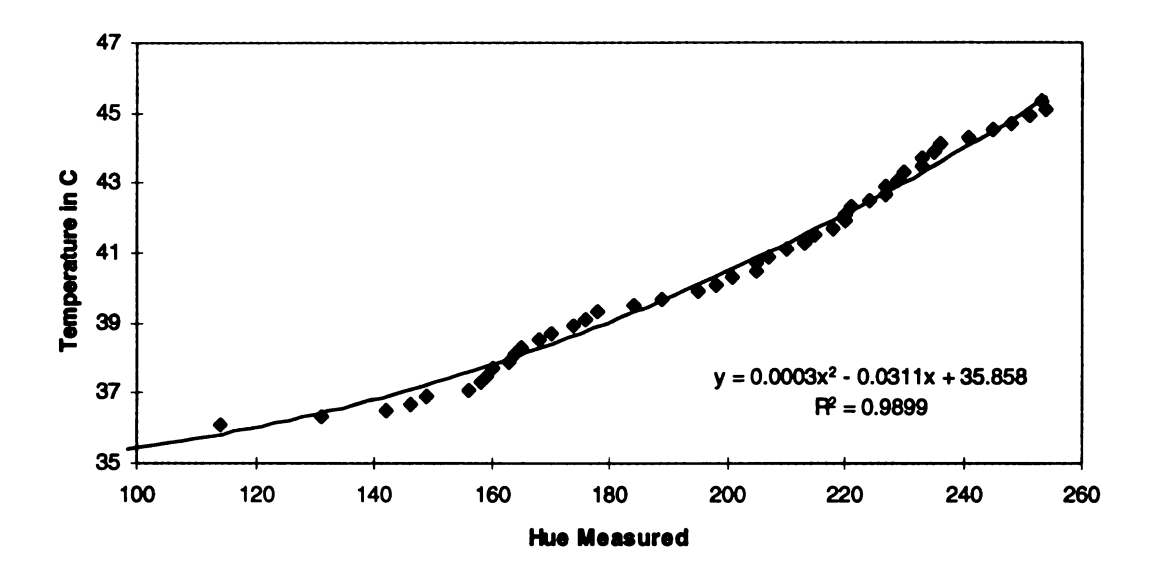


Figure 9. Polynomial fit for the calibration data of Liquid crystals

After the calibration of liquid crystals, the experiments with the electrically heated blade were conducted. The flat blade coated with the calibrated liquid crystals was connected to an AC power source through a variac and is placed in the test section of the wind tunnel. By adjusting the variac and measuring the voltage and the current with help of a voltmeter and an ammeter connected to the power source, the power supplied to the blade is controlled. Under steady state conditions the temperature on the surface was measured using the calibrated liquid crystals. The velocity distribution at six streamwise locations on the blade was measured using a total pressure probe and a factory calibrated HHP-102A electronic manometer, which is capable of providing both the total pressure and the static pressure at a particular location to 0.2% accuracy. Also, a specially constructed thermocouple probe whose tip is 0.0762mm, was used for measuring the temperature gradients above the surface of the plate to determine the local heat transfer coefficient.

Using the variac, the desired heat flux is provided to the plate and calibrated liquid crystals are used to provide the steady state surface temperatures with a precision of 0.01°C and with an accuracy of 0.1°C. The air temperature was measured using a thermocouple probe which traversed in a direction normal to the surface of the plate at increments down to 0.2mm with an accuracy of 0.15°C.

The blade is analyzed as a flat blade taking into account the curvature effect of the leading edge and the stagnation region that develops due to the blunt leading edge as shown in Figure 10. The curvature of the blade is accounted for by measuring the arc length of the leading edge and flattening it out. After that, the boundary layer thickness that is created due to the blunt nose effect is calculated and the virtual length (corresponding to the equivalent boundary layer thickness for a flat blade) is added to the existing flat section and the arc length of the leading edge to give the virtual starting point of boundary layer development. This correction in the leading edge was necessary in order to account for the stagnation and curvature effect at the leading edge of the blade.

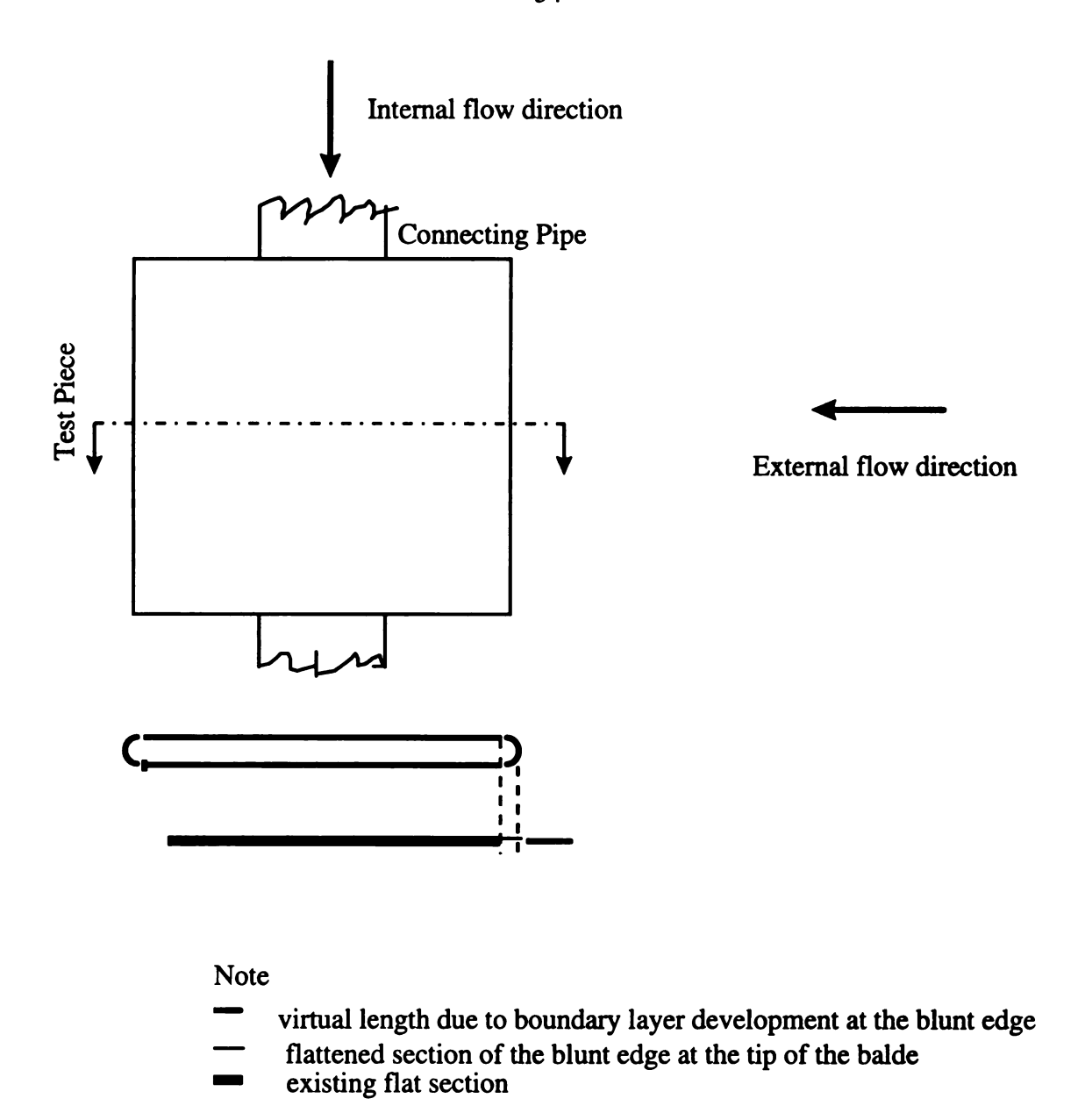


Figure 10. Corrected Configuration of the blade

The velocity and temperature profiles measured at the dimensionless location x/L = 0.72, using the procedure outlined above is shown in Figures 11 and Figure 12. In Figure 11, the

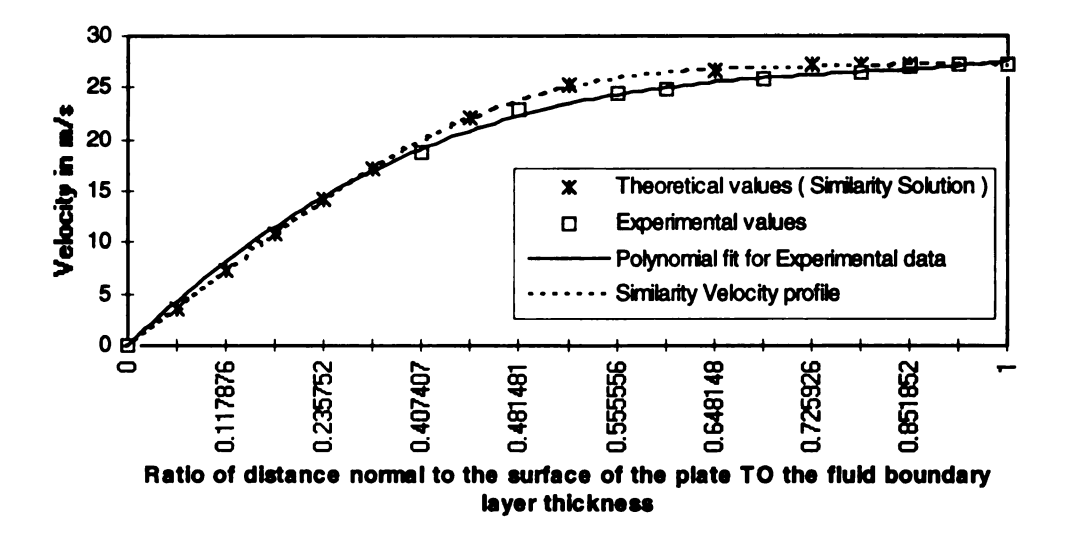


Figure 11. A typical velocity profile on the electrically heated flat blade (At the location x/L = 0.72, from the leading edge)

velocity profile measured using the experimental data is compared against the velocity profile of the similarity solution for laminar flow. This shows that the corrected virtual length analysis discussed previously agrees well with the flat blade assumption.

In Figure 12, the measured temperature profile generated is shown. This is compared against the temperature profile that Prolhac used while obtaining the integral solution for the energy equation. The linear temperature profile very close to the wall is typically used for computing the temperature gradients at various streamwise locations on the blade surface which are then used to compute the local heat transfer coefficient using

$$h_{ext} = -(k dT / dy)_{ext} / (T_s - T_{amb}).$$

Using this the external local Nusselt Numbers are calculated $Nu_{x,ext} = h_{ext} x/k_{ext}$.

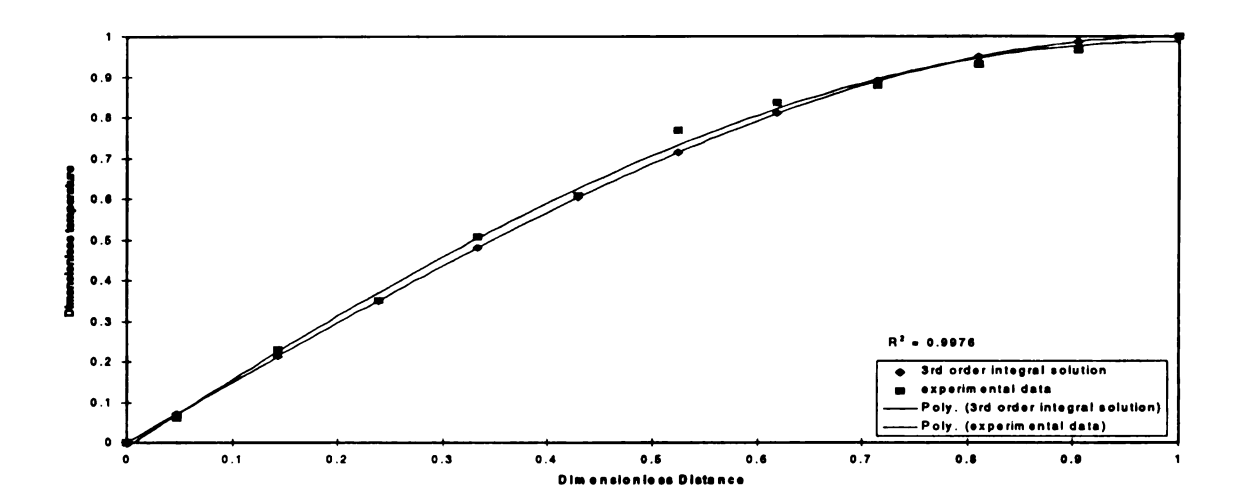


Figure 12. A typical temperature profile over the electrically heated blade surface (At the location x/L = 0.72, from the leading edge)

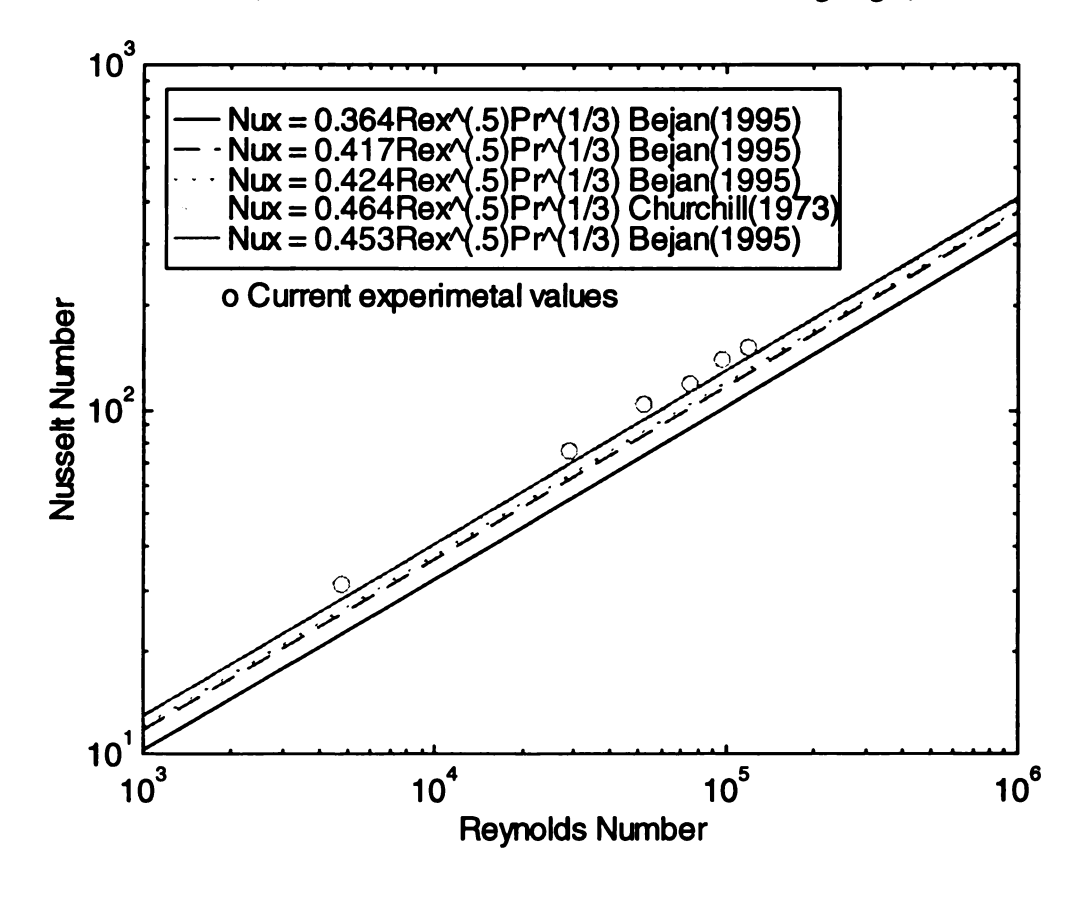
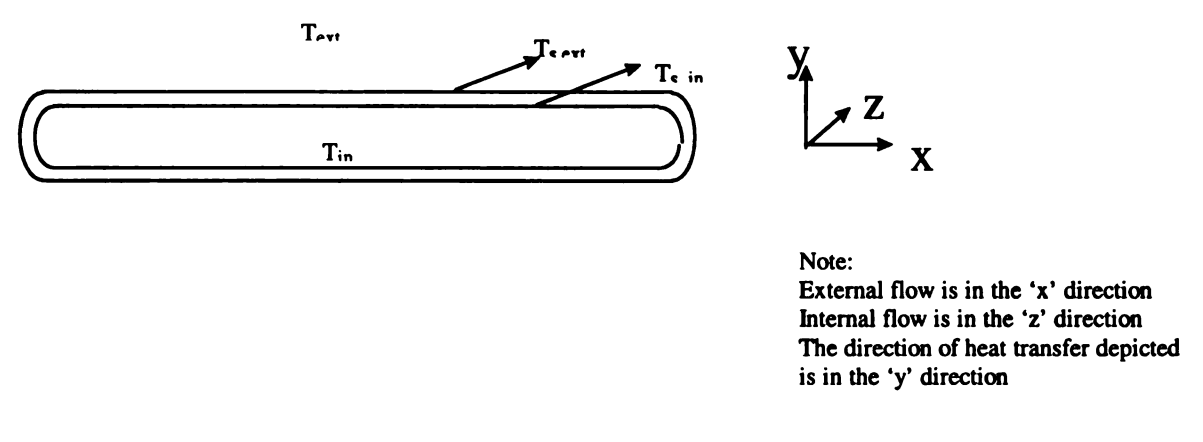


Figure 13. Local Nusselt Number versus Local Reynolds Number for an Electrically heated plate

Figure 13 shows the external Nusselt Number plotted against the external Reynolds Number on a log-log scale. The dashed lines in this figure indicate the theoretical predictions, and the 'o' represents the experimental data that have been generated using the procedure outlined above. This demonstrates that the Nusselt Number varies as 1/2 power of the Reynolds Number which is consistent with the existing theories for laminar flow over flat surfaces.

These experimental results clearly show that the above procedure can be employed to accurately determine external Nusselt Numbers. The aims of this phase of the project were to establish confidence in the liquid crystal surface thermography technique and to determine the relation for the external side heat transfer for the model blade.



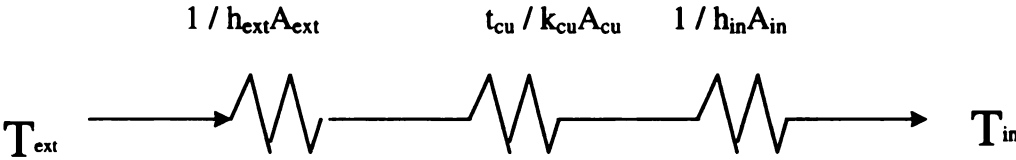


Figure 14. Illustration of the electrical analogy model set up to compute 'hin'

Having established a standard procedure for evaluating the external heat transfer coefficient, a similar set of experiments was conducted on an internally heated/cooled blade. These experiments involve heating the blade internally by passing either dry steam or hot air through the blade and cooling by the external flow of air in the wind tunnel. The configuration being tested is similar to the electrically heated blade. The blade that was studied is a single pass rectangular cross sectioned blade with a curved leading edge made out of copper.

The external heat transfer coefficient determined by the above procedure is used to evaluate the internal heat transfer coefficient using the heat resistance model as modeled in Figure 14. The following equation is used to compute the heat transfer coefficients on the internal side once the external heat transfer coefficient is known.

$$Q = (T_{in} - T_{ext}) / (1 / h_{ext} A_{ext}) + (t/kA)_{cu} + (1/h_{in} A_{in})$$

The only unknown in the above equation, h_{in}, is evaluated after determining 'h_{ext}' from the procedure outlined above.

The measurements and data reduction made on the single pass internally cooled blade are shown in Figures 15 through 18 for different experimental runs. Figures 15 and 16 show the temperature profiles measured at a distance of 4.194cm from the corrected leading edge of the plate for hot air case and super heated steam case respectively. These measurements have been compared with the dimensionless temperature profile for a flat plate analysis. From these figures, it is clear that the temperature profiles measured agree well with the theoretical predictions of the 3rd order integral solution.

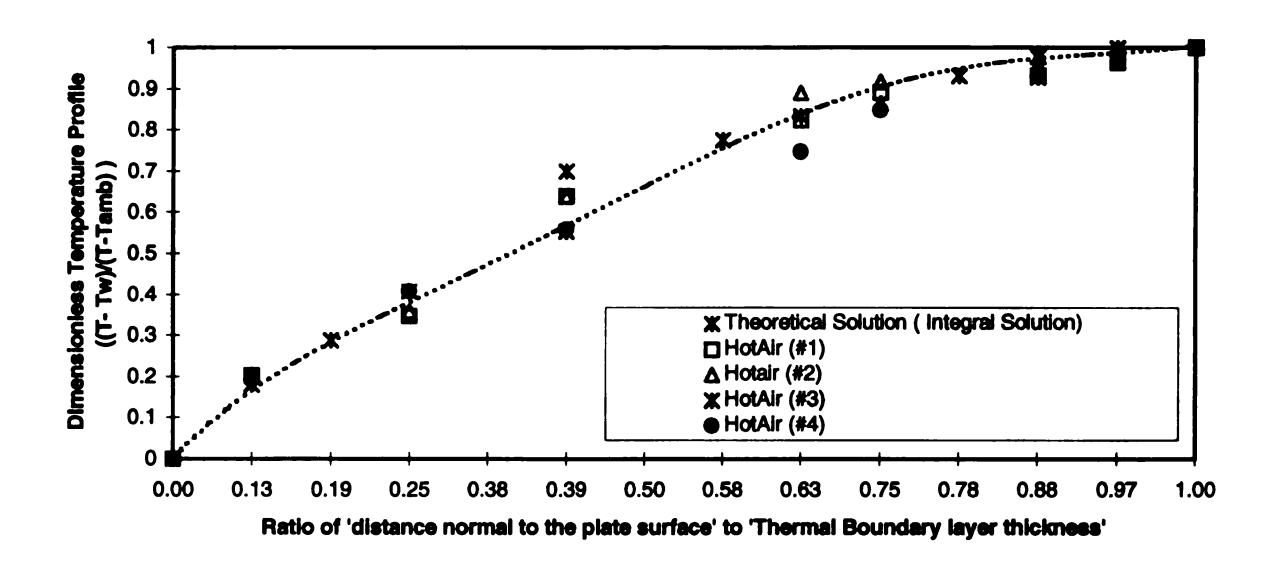


Figure 15. Dimensionless Temperature Profile at 4.194cm from the leading edge with hot air being circulated internally.

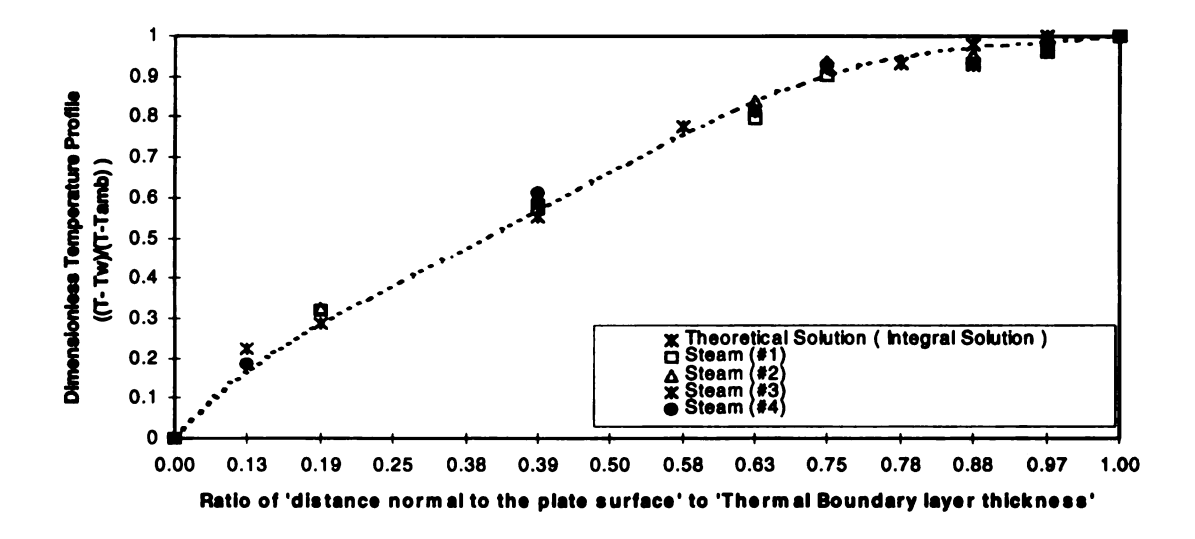


Figure 16. Dimensionless Temperature Profile at 4.194cm from the leading edge with super heated steam being circulated internally.

Once these temperature profiles were measured, the external Nusselt Numbers were evaluated, using the gradient of the temperature profile at the wall. And using these local

external Nusselt Numbers, the local internal Nusselt Numbers have been evaluated using the procedure discussed earlier.

The average internal Nusselt Number versus Reynolds Number relationship is shown in Figure 17. This is compared with the theoretical predictions for a turbulent flow within a rectangular duct. From this figure, it is clear that for the configuration under study, the internal Nusselt Numbers for both the hot air and the super heated steam cases vary as 4/5th power of the Reynolds Number which is expected for a turbulent duct flow. And as a further result, for identical Reynolds Number flows, the heat transfer coefficient would be higher for fluids which have a higher thermal conductivity, in this case steam.

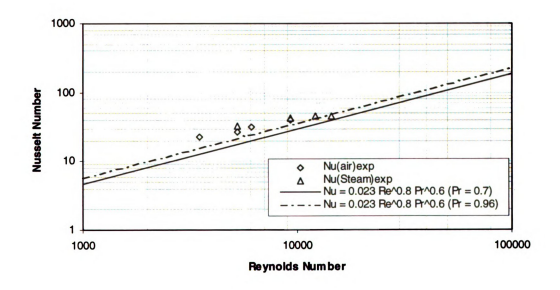


Figure 17. Average Internal Nusselt Number versus Average Internal Reynolds Number

Figure 18 shows the internal Nusselt Number as a function of dimensionless distance along the internal fluid flow direction. It can be seen that the experimentally averaged Nusselt Numbers for both the hot air and superheated steam case lie in the flattened part of the curve indicating that the flow is close to reaching the thermally fully developed state. Since the instrumentation available, cannot determine the internal temperature profile in the experiments, an analytical model with the experimental boundary conditions was developed using ANSYS 53 analysis tool, and the results of this analysis is presented in Figures 19 through 22.

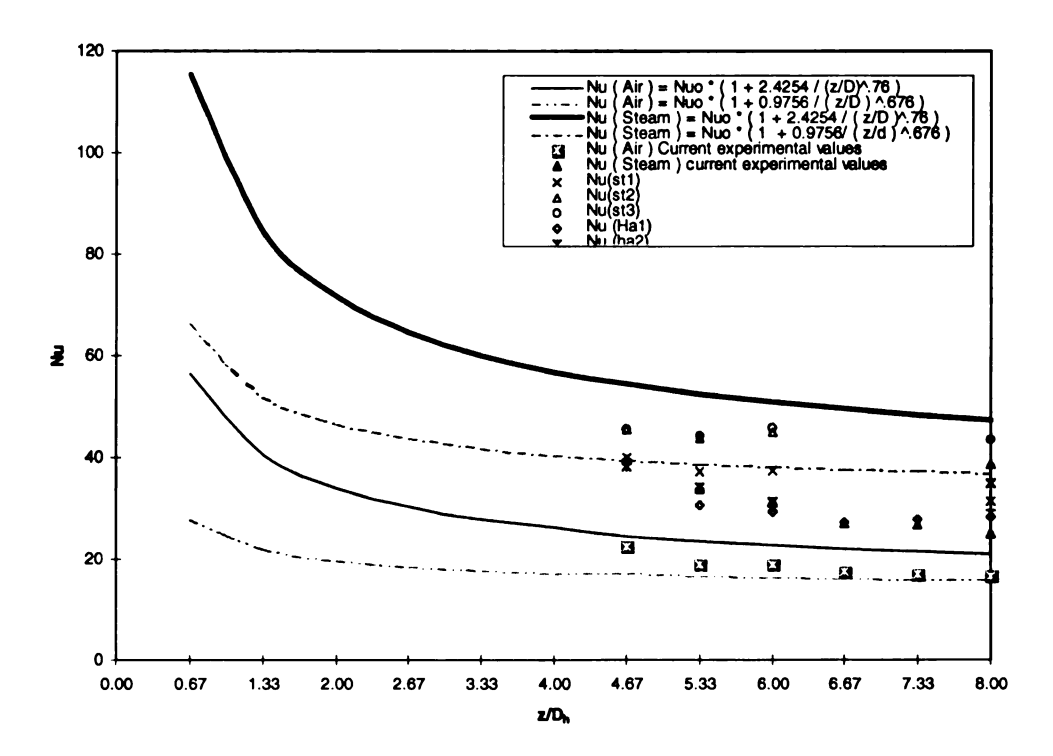


Figure 18. Local Nusselt Number versus dimensional distance in the direction of internal flow

), : es.		

Figure 19 shows the numerical model built for this purpose using ANSYS 53. This 3D model is composed of 13200 3D Flotran142 type elements. The boundary conditions that were imposed on this were the results that are obtained from the experiments. A constant heat flux boundary condition was imposed on the exterior surfaces of the flat test section, and the measured experimental temperatures were imposed on the inlet and the outlet along the internal flow direction. Adiabatic boundary conditions are imposed on the entrance and exit pipe sections of the test blade. Also at the inlet and outlet, measured velocity and pressures are imposed as the boundary condition. All along the boundary, a no slip velocity boundary condition is imposed.

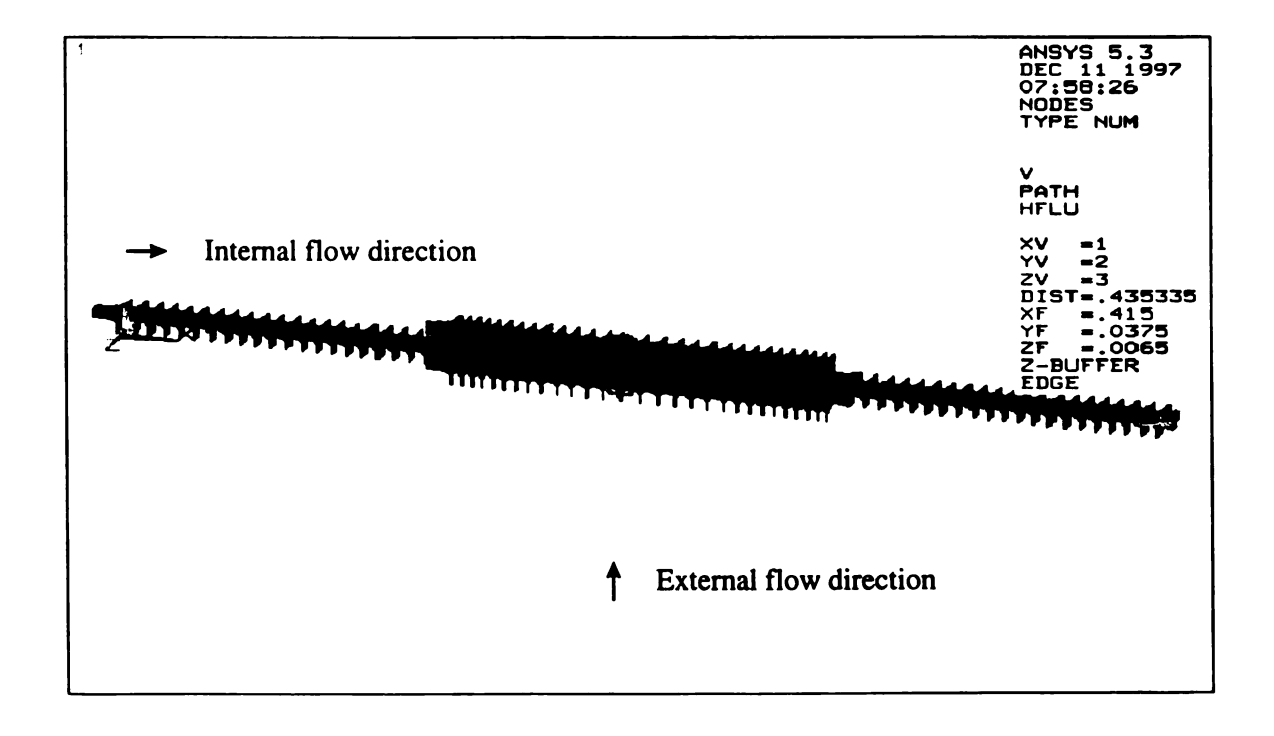


Figure 19. ANSYS 3D Numerical Model that was built to verify the experimental assumptions

Figure 20 shows the velocity profile along the centerline of the test blade at z/Z=0.5, y/Y=0.5. The velocity profile along the cross section at this location is a parabolic fully developed profile as shown in the figure, with the maximum velocity occurring at the mid section of the cross section. At either ends of the cross section, the velocity profile does not have the same smoothness as the mid sectional velocity profile because of the geometry of the blade being investigated. This irregularity in the velocity profile did not affect the results in the experiments as the experimental data were measured in the sections where the velocity profile has the parabolic behavior. This provides the confidence in the assumption that the flow was fully developed at the measurement locations.

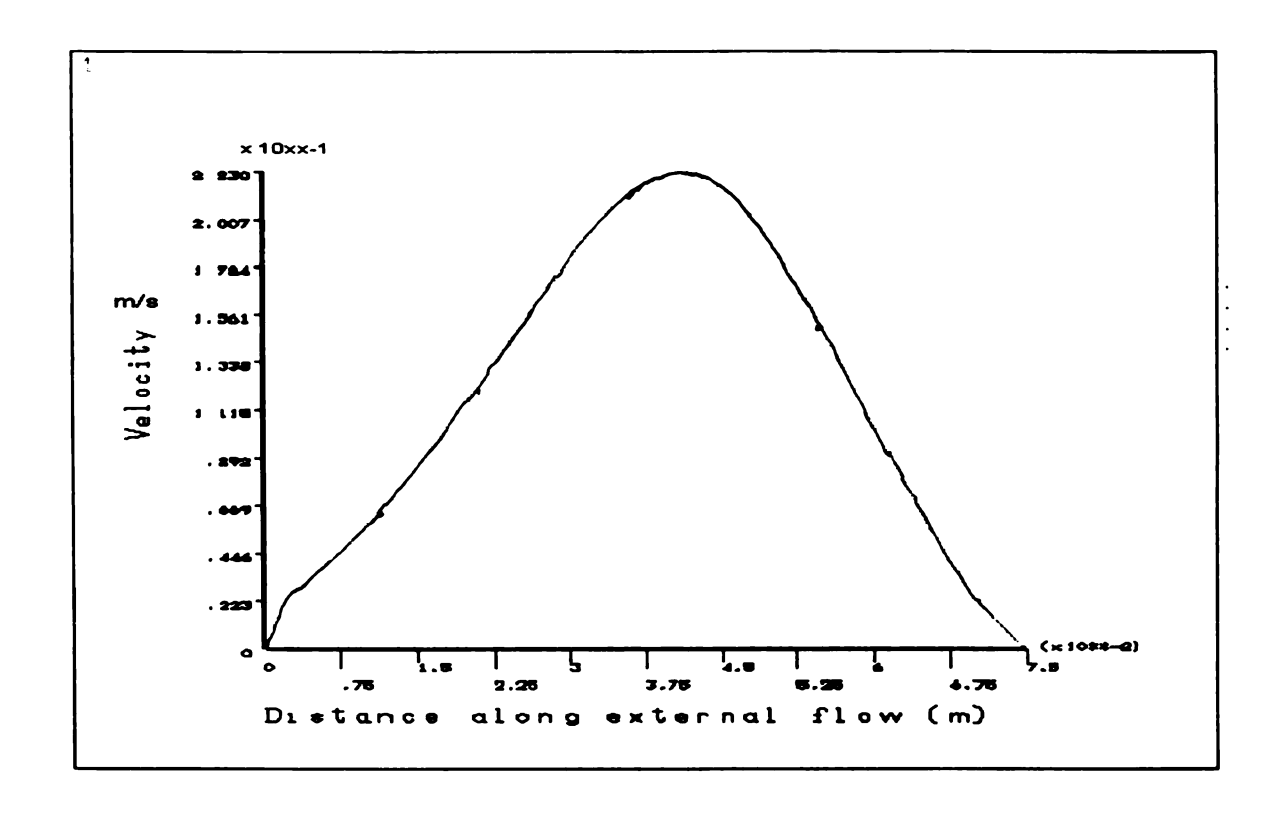


Figure 20. Computed velocity profile of the internal fluid at the center cross section in the external flow direction

In Figure 21, the temperature profile that is obtained from the steady state analysis of the numerical model at the same cross section, as discussed above, is shown. This shows that the temperature profile is flat along the cross section at the specified location where measurements were made, with no spikes in between which justifies the assumption of a thermally developed flow. Figures 20 and 21 show that the internal flow is close to being hydrodynamically as well as thermally fully developed.

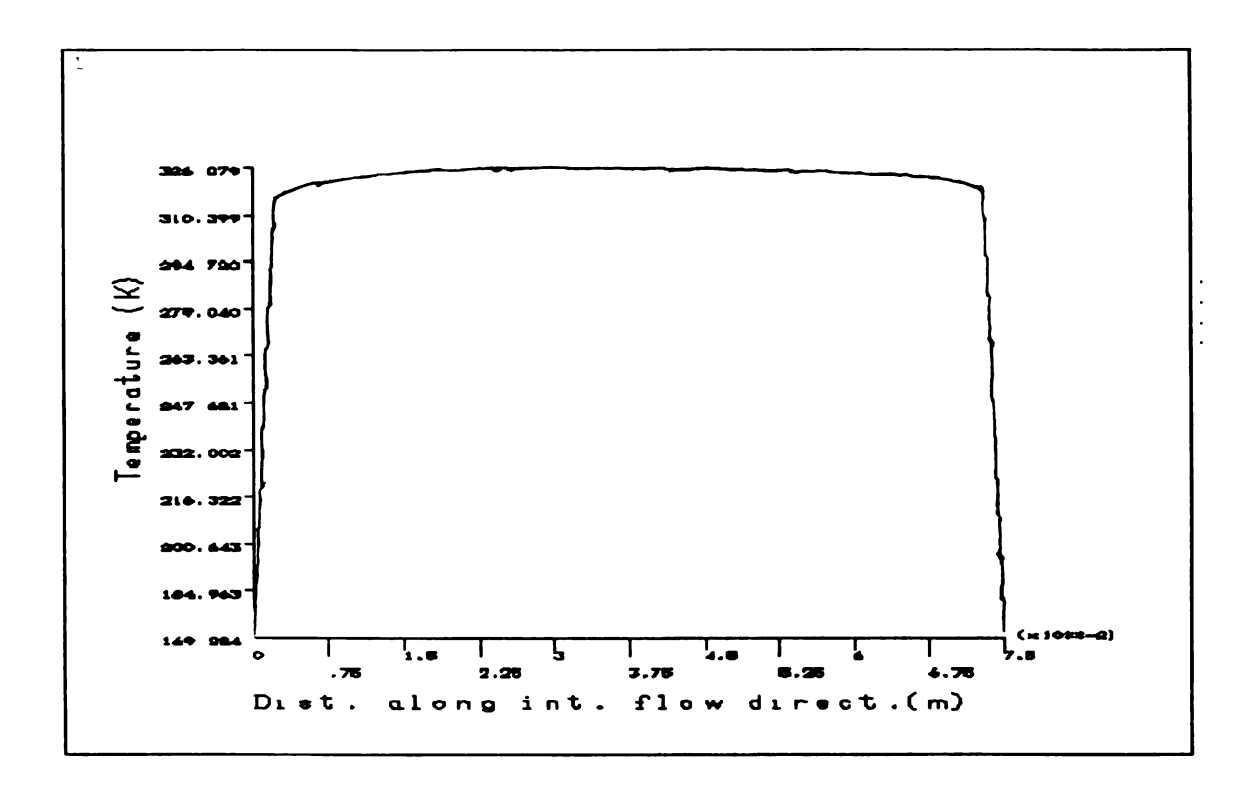


Figure 21. Temperature Profile of the internal fluid across the middle along the external flow direction

Figure 22 shows the temperature profile of the fluid along the central line of the internal flow (y/Y = 0.5, z/Z = 0.5). This figure shows that the temperature drop of the internal fluid along the flow direction is close to being linear in the section of the model blade which is inside the test section of the wind tunnel, which provided the necessary justification for the experimental assumption that the internal temperature profile is linear from the inlet to the outlet section of the test blade. Near the inlet and the outlet sections, there is a deviation in temperature profile from the linearity because the flow is suddenly being expanded/constricted to fit into the inlet/outlet pipe fixture. These two regions did not affect the results as they were outside the test sections of the wind tunnel.

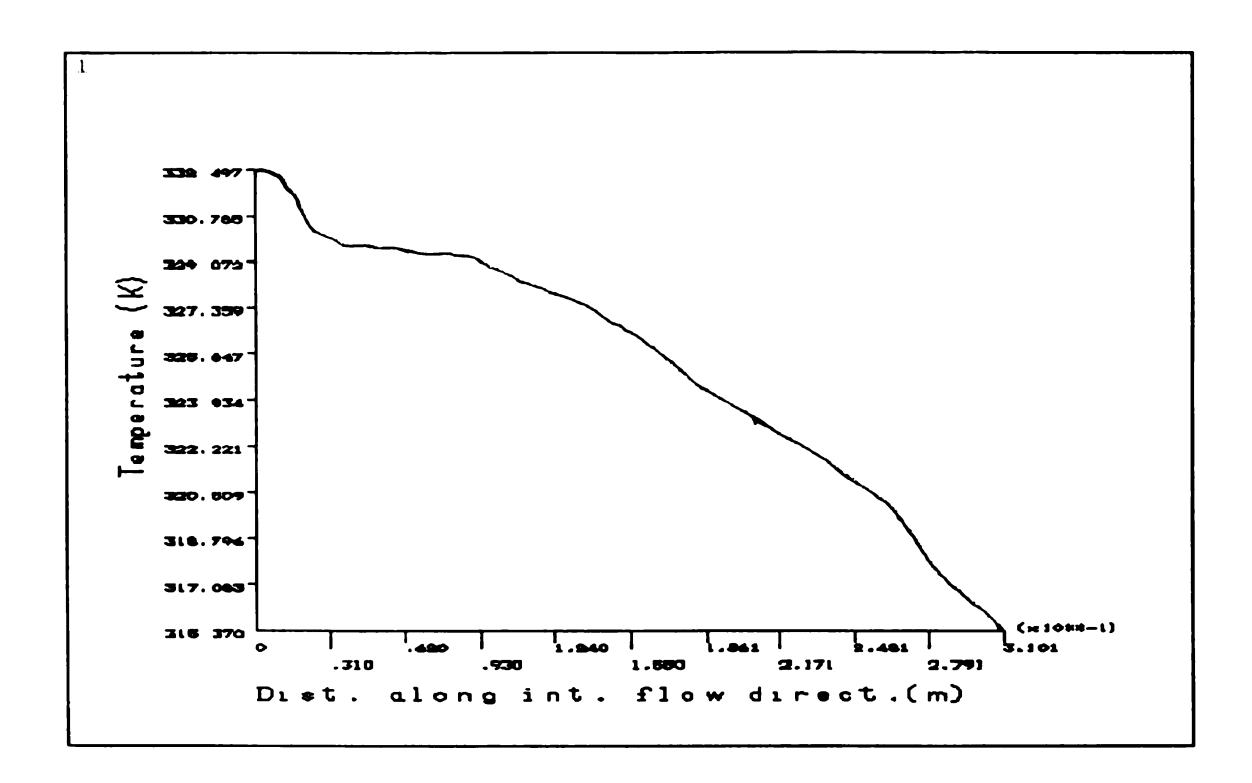


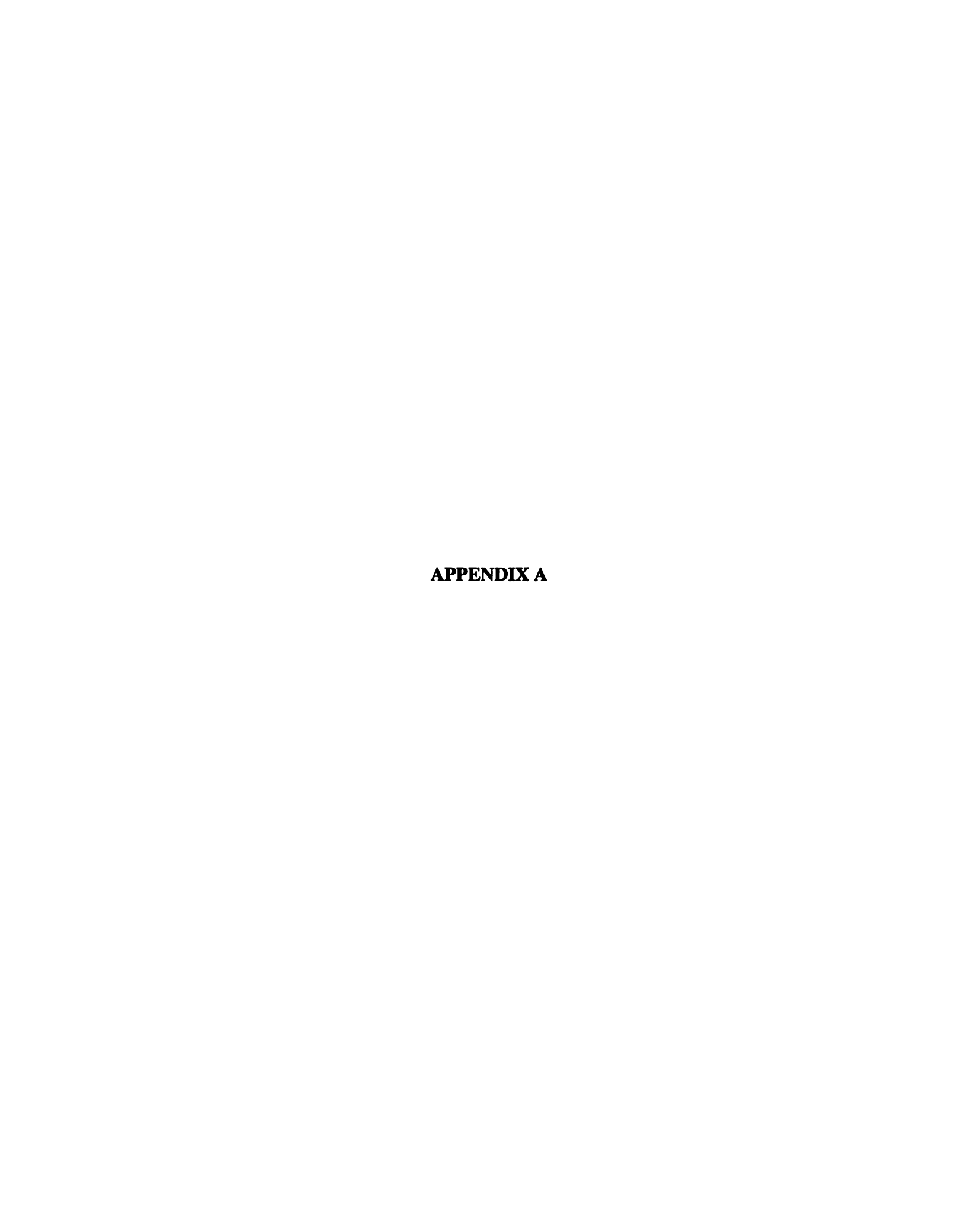
Figure 22. Temperature Profile of the internal fluid from inlet to exit

The measurement uncertainty analysis on the experimental parameters was carried out based on Moffat(1992). The uncertainties due to mass flow rate of air, velocity of air, external Nusslet Number, internal Nusslet Number and the heat energy delivered are estimated to be .0225 gm/s, 0.069m/s, 11.1431, 4.09 and .9W respectively. The uncertainty of the liquid crystal temperature measurement was 0.2°C.

CONCLUSIONS

Distributions of external and internal heat transfer coefficients and Nusslet Numbers for hot air and superheated steam along the single pass blade was obtained in the specially designed wind tunnel using the liquid crystal technique. Several conclusions can be made from this study

- Application of the Liquid Crystal Technique for determining the temperature distribution and hence the heat transfer distribution on a one pass blade configuration presents an attractive and efficient way of obtaining experimental data with low uncertainty values. This technique also provides a way of measuring data in a manner that is non obstructive to the flow.
- The experimental analysis approach of unwrapping the blunt leading edge into a
 virtual sharp edged flat blade, in order to correct for the leading edge effect, for this
 blade geometry agreed well with the data analysis.
- The use of ANSYS53 as a numerical tool to justify the experimental assumptions
 worked well for the experimental velocity as well as the temperature profiles. This
 analysis provided the necessary confidence in the experimental approach adopted.
- The internal Nusselt number comparisons between steam and air indicate that they both vary as the 0.8 power of the Reynolds Numbers. Since the heat transfer coefficient of the fluid is directly proportional to the thermal conductivity of the fluid, and because of steam's higher thermal conductivity and specific heat capacity, we would expect a much higher heat transfer from steam compared to air. At higher pressures and temperatures, this effect would be more pronounced. As the dimensionless numbers indicate, for the same kind of flow conditions, steam has a much higher heat transfer coefficient compared to that of air. All these experimental results look promising towards using steam as an alternative for air for the cooling of the turbine blades.



Appendix A

Experimental Apparatus

The wind tunnel designed and constructed for this purpose is powered by a Dayton Blower. The tunnel test section is about 1.2m long (including the entrance length) and is made up of multiple interchangeable sections made of clear plexiglass, to allow optical measurements to be made. The model blades are mounted in the flow of the stream in a section which is 0.3m long, upstream of the blade is an entrance length section which is connected to a honeycomb structure at the inlet of the tunnel for straightening the flow in the tunnel. The velocity profile of the flow with the honeycomb at the entrance, is shown in the following figures. The velocities at different locations were measured using a pitot probe and hand held manometer.

Figures A1, A2 and A3 show the velocity profile across the test section with different entrance lengths of 0.9m, 1.2m, and 2.1m respectively. The velocity profiles shown in these figures indicate that the flow is fully developed and laminar, in all three cases. The flow also appears to be flat at the center portion of the test section, which is were all the temperature gradient and pressure gradient measurements are made.

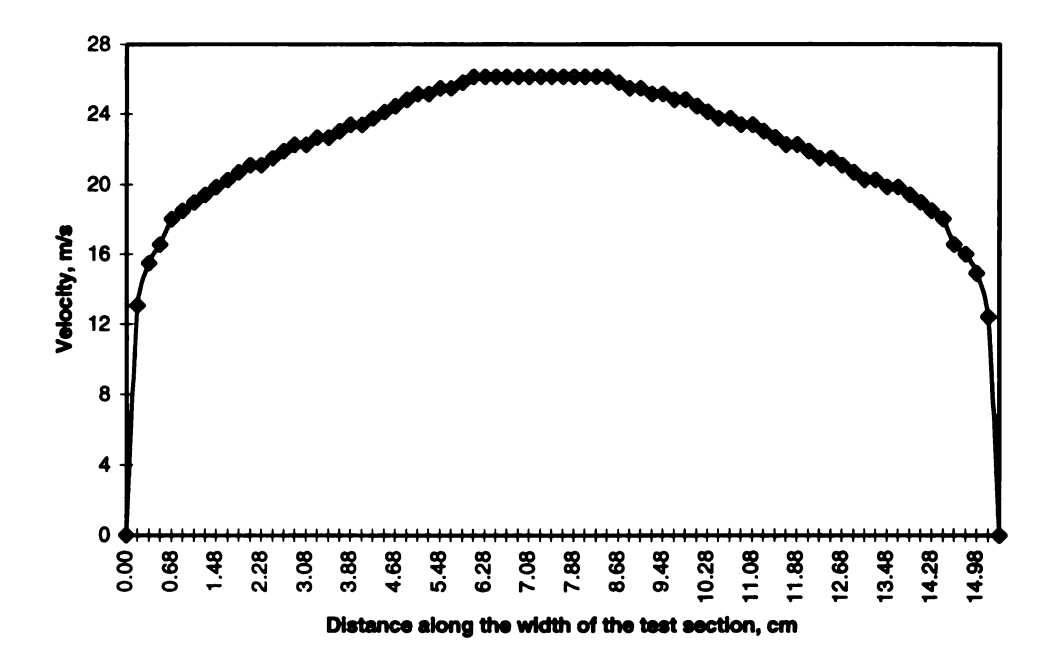


Figure A1. Velocity profile of the air flow across the width of the test section for an entrance length of 0.9m.

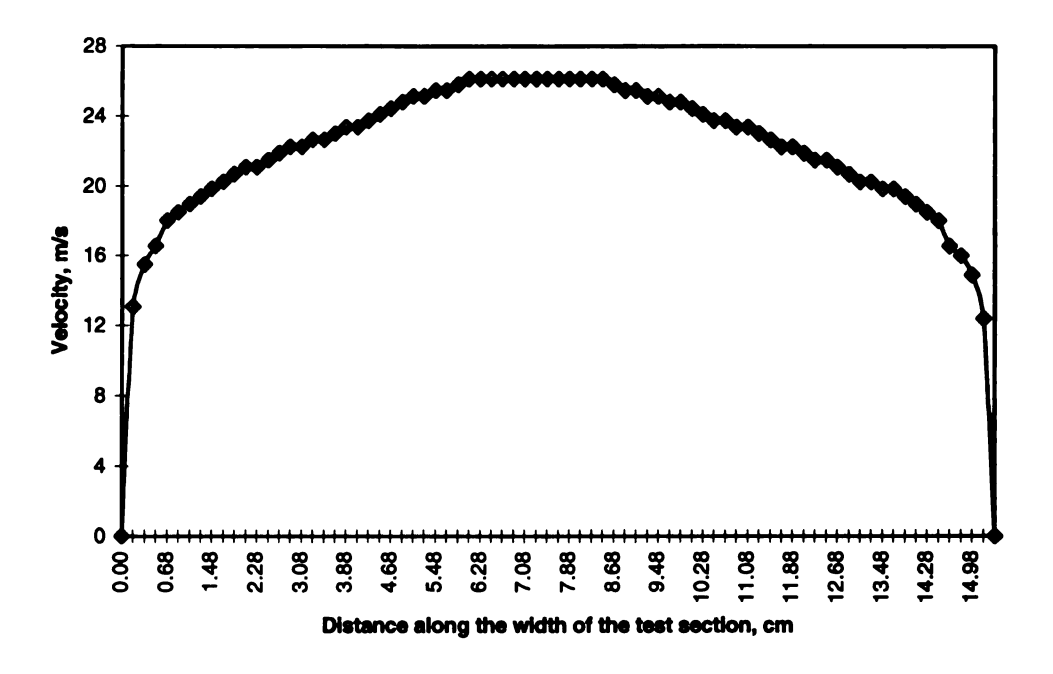


Figure A2. Velocity profile of the air flow across the width of the test section for an entrance length of 1.2m.

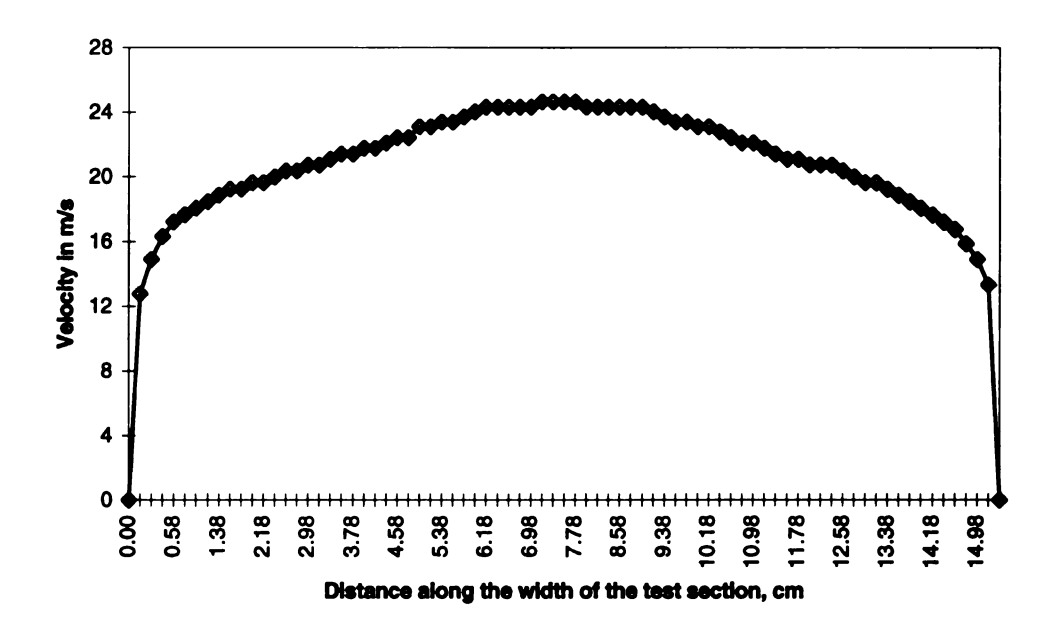


Figure A3. Velocity profile of the air flow across the width of the test section for an entrance length of 2.1m.

Figures A4, A5 and A6 show the velocity profile in the test section, from top to bottom, with different entrance lengths of 0.9m, 1.2m, and 2.1m respectively. The velocity profiles shown in these figures again indicate that the flow is fully developed and laminar. In addition to this, it is flat at the center of the test section which is where the temperature and pressure gradients are measured.

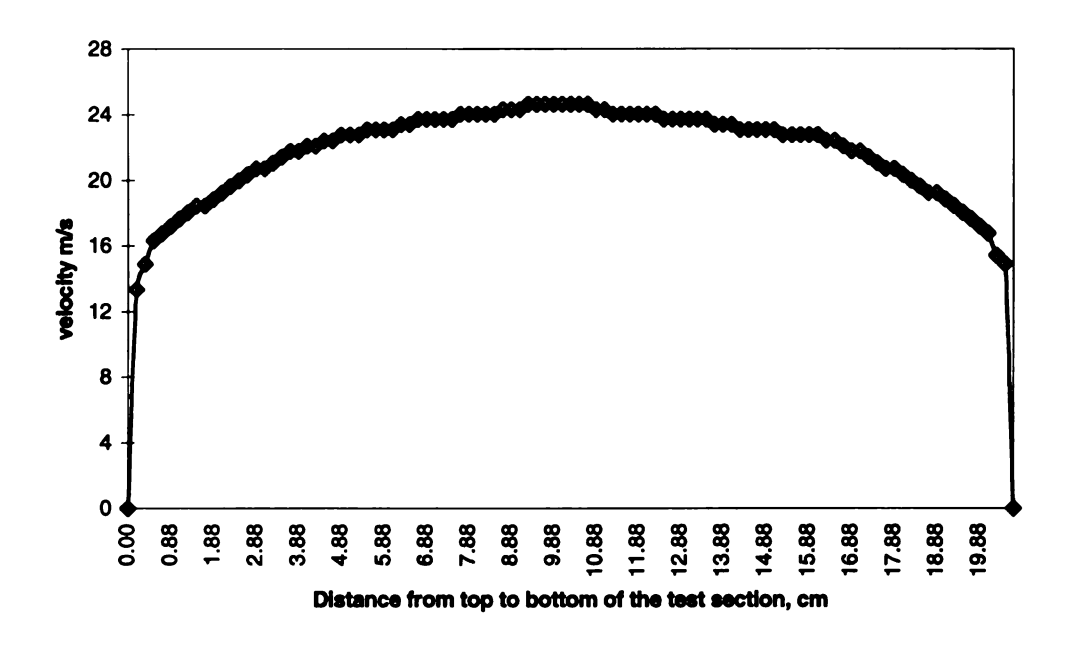


Figure A4. Velocity profile of the air flow from top to bottom of the test section for an entrance length of 0.9m.

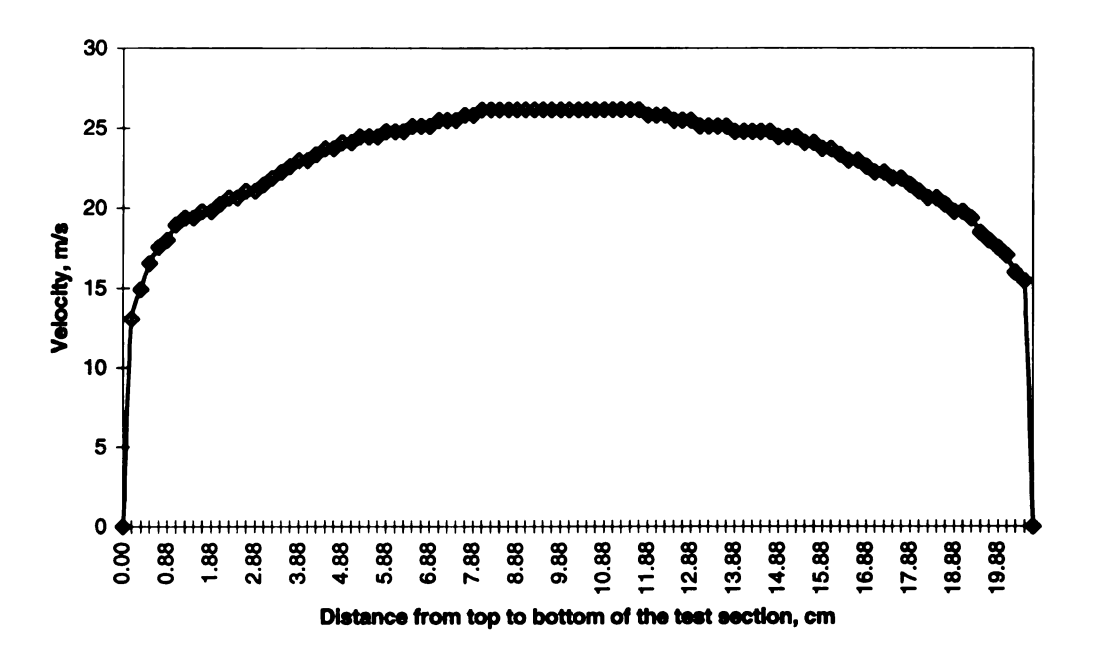


Figure A5. Velocity profile of the air from top to bottom of the test section for an entrance length of 1.2m.

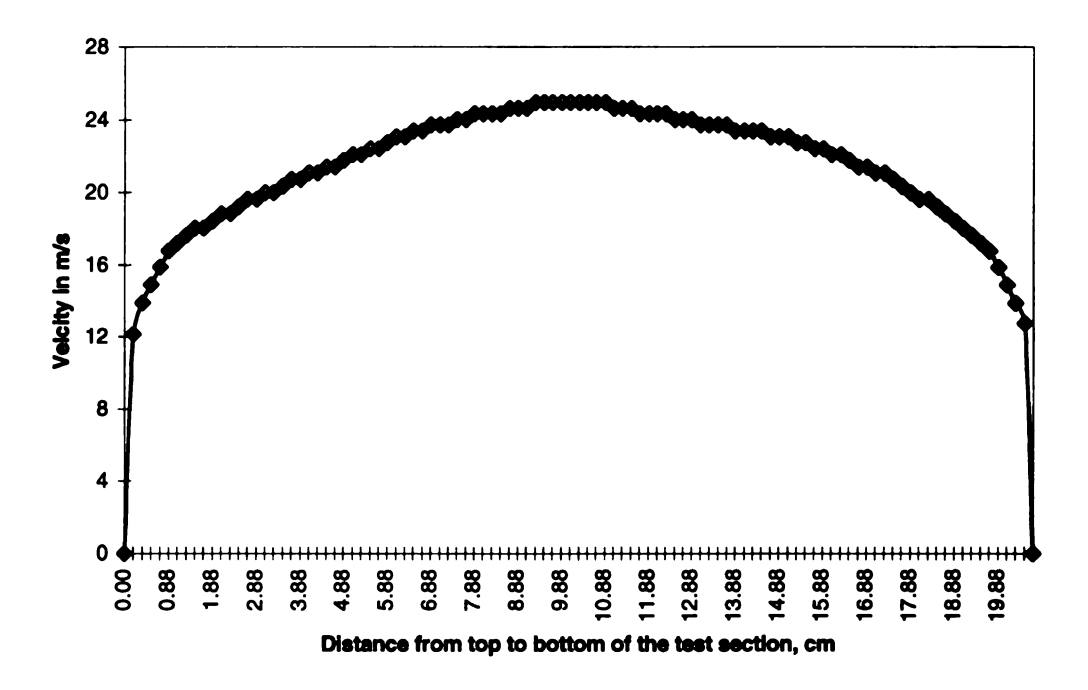
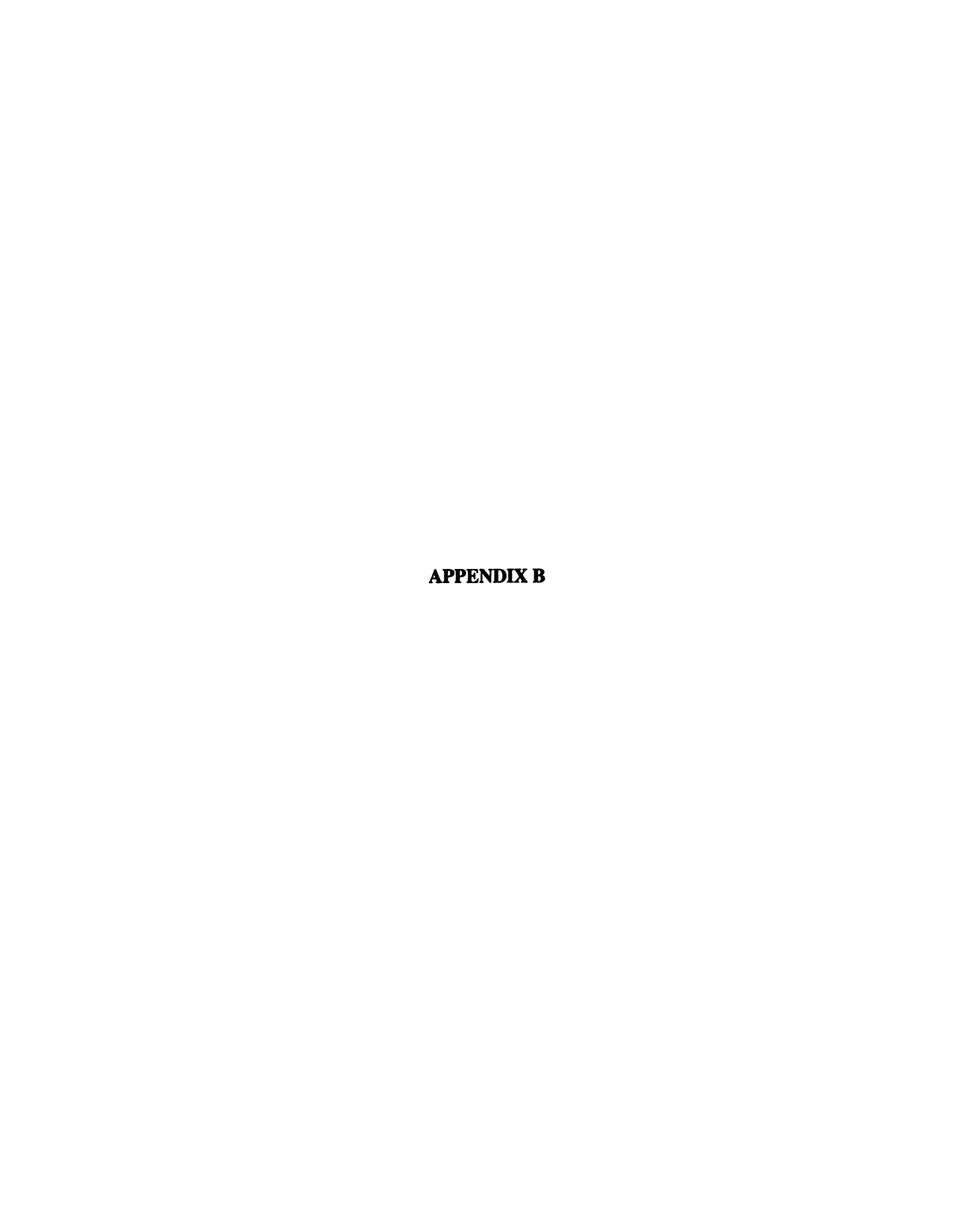


Figure A6. Velocity profile of the air flow from top to bottom of the test section for an entrance length of 2.1m.

It is clear from the above figures that the entrance lengths do not affect the flow field within the test section. Because of this, the entrance lengths for all measurements in the experiments were chosen as 0.9m arbitrarily. Furthermore, since the center of the test section indicated that there were no pressure gradients at that section, the measurements made above the model blade were solely due to the blade.



APPENDIX B

LIQUID CRYSTAL HEAT TRANSFER MEASUREMENT TECHNIQUE

Introduction

In 1888, an Austrian botanist, Friedrich Reinitzer, observed that certain organic compounds appeared to possess two melting points, an initial melting point that turned the solid phase to a cloudy liquid and a second melting point at which the cloudy liquid turned clear. Further research revealed that an intermediate phase, or "mesophase" did indeed exist between pure solid phase and pure liquid phase of some organic compounds. Reinitzer termed this phase a "liquid crystal phase". Since his work, a great deal of research concerning the structure of liquid crystals has been carried out resulting in the classification of liquid crystals into one of three categories: smetic, nematic, or cholesteric; the particular category being determined by the molecular structure.

Liquid Crystals are frequently used in applications for measuring the local surface temperature. This type of thermometer enables the surface temperature to be determined over a complete area and, in the absence of lateral heat conduction, allows the local heat transfer coefficient to be calculated. This measured heat transfer distribution can be used directly in the design of components or in the development of flow predictive methods.

Temperature sensitive liquid crystals provide one of the most convenient and accurate ways of measuring surface temperature distributions. They have been used both in transient and steady state heat transfer measurements. One of the basic assumptions considered in all these applications is that the crystal coating is hydraulically smooth and, geometrically and thermally very thin. Under these conditions, the temperature sensitive coating is non-intrusive.

Thermochromic Liquid Crystals

Liquid Crystals are substance which in certain phases have the mechanical properties of liquids but the optical character of a crystal. Under specific conditions, the optical properties can be dependent on physical factors such as the stress, electrical, magnetic or temperature fields. Substance which exhibit liquid crystal behavior with temperature changes are known as thermotropic. These organic molecules are generally of the order of 20-30 angstroms long and about 5 angstroms in diameter. On heating, from the solid state, the materials melt but long range order is sustained by intermolecular forces until the final melting temperature to the isotropic state. Whilst in the liquid crystal mesophases, the molecular anisotropy causes long range ordering of molecules which gives rise to anisotropy in physical properties such as refractive index, conductivity and viscosity. This ordering of molecules traces a helix, and this structure becomes optically active when the pitch of the helix is of the order of the wavelength of the incident light. A change in the pitch with temperature is responsible for the change in surface color on heating.

A variety of externally applied fields including electrical, magnetic, shear, pressure and thermal fields have been found to produce a change in the optical properties of liquid crystals. Cholesteric liquid crystals, as the name implies, are formed from the esters of cholesterol. The property of interest, from the heat transfer point of view, of the cholesteric type liquid crystal concerns its response to temperature. Over a known, reproducible range of temperature, the "event temperature range", the cholesteric liquid crystal will progressively exhibit all colors of the visible spectrum as it is heated through the event temperature range. The phenomenon is reversible, repeatable and with proper care, color can be accurately calibrated with temperature.

At present, the liquid crystals are commercially available with event temperature ranging from a few degrees below zero t several hundred degrees Celsius. Liquid crystals can be obtained with event temperature spans as small as 1°C to as large as 50°C.

Pure liquid crystals, although exhibiting brilliant colors, pose several problems from the point of view of usage. Once applied to a specimen, the pure liquid crystals deteriorate rapidly with age permitting only a few hours of experimentation. They are also susceptible to contamination with marked alteration in their performance. Further, the detection of temperature by change of color is strongly influenced by viewing angle.

Many of the problems associated with the use of pure cholesteric liquid crystals have either been eliminated or greatly reduced through an encapsulating process developed by National Cash Register Company. The encapsulated liquid crystals are coated with gelatin in a polyvinyl alcohol binder. In addition to extending the life of the liquid crystals, the encapsulation also greatly reduces the variation of color due to the viewing angle. Encapsulated liquid crystals can be obtained as precoated on a blackened substrate of paper or mylar, or in water based slurry. For our experiments, the encapsulated liquid crystals were obtained in slurry form which allowed manual coating of the specimen surface using an air brush.

Coatings

In all the work that is detailed in this report, the liquid crystals were applied in an encapsulated form. Care must be taken to ensure that the surface is fully dry before the crystal mixture is applied. A thin coating (approximately 20µm) is developed by spraying many thin coats with interim drying using an air heater. This coating is applied over a thin coating of black paint. This allows an enhancement of the color display contrast. Also the black substrate insures that all light transmitted through the liquid crystal film is absorbed and, therefore, is not reflected to compete with the desired signal. An overall layer of between 20-30µm is sufficient since the response does not improve with increased thickness.

Time Response

The accuracy of the measured temperature during a transient test depends on the rate at which the liquid crystals can respond to the surface temperature change. The earliest measurement of the time response was made by Parker who investigated a material derived from cholesterol. Ireland and Jones also measured the time response. These experiments showed that the delay between the time at which the surface reached the steady state color display temperature and the occurrence of the color display was no more than a few milliseconds. Bonnet investigated the time constant of several liquid crystal materials by pulsing an indium tin oxide heater on a glass substrate. He used a bridge circuit to monitor the resistance of the heater and hence record the temperature of one surface of a covering 10-15µm layer of encapsulated liquid crystals. He was able to show that time constant for a typical chiral nematic mixture with color display close to room temperature is about 10ms whereas a room temperature cholesteryl ester mixture has a time constant of over 100ms. This led to the conclusion that the actual time delays observed during heating tests are shorter than the measured time constants. (Ireland P.T. (1992)

Cholesteric liquid crystals have been employed in a number of interesting applications over the past several years. In the field of non destructive testing, Dowden (1967) used liquid crystals to check for irregularities in the bonded structures, to observe regions of overheating on electronics equipment. Woodmansee (1968) used these liquid crystals to

check for flow blockages in heat exchangers, as crack detectors in aircraft structure, and to check the effectiveness of windshield heaters, to name a few typical applications. In the medical field, Crissey (1965) used cholesteric liquid crystals to observe surface blood flow patterns in humans and as a diagnostic tool for detection of breast cancer. Cook (1971) used cholesteric liquid crystals to study the characteristics of ultrasonic beams.

Several investigators have employed liquid crystals as a temperature transducer in engineering heat transfer studies. Raad and Myer(1971) used liquid crystals to observe nucleation sites in a study of pool boiling. Ennulat and Fergason(1971) employed a liquid crystal film as the display device in a non contacting thermal imaging system. Maple(1972) studied the transient and steady state temperature fields that develop on the exterior of an active sonar transducer by coating the surface of the transducer with liquid crystal. Cooper and Groff (1973), Katz and Cooper (1973), and Cooper and Petrovic (1974) employed liquid crystals coated on a thin mylar sheet to observe temperature fields produced by resistively heated, radio frequency, and cryosurgical cannulas, respectively.

The use of cholestric liquid crystals in wind tunnel experiments was first investigated by Klein in 1968. McElderry(1970) in an investigation similar in principle to the one conducted by Klein, used unencapsulated cholesteric liquid crystals as a means of determining boundary layer transition on a flat plate placed in supersonic air stream.

Hippensteele et.al (1981) investigated the performance of heat transfer measurements using liquid crystal coatings on a commercially available composite sheet and found it to

provide a simple, convenient, accurate and low cost measuring device for use in heat transfer research. Simonich and Moffat (1982) used liquid crystals to map heat transfer contours quickly and easily. They conducted the tests to qualify the technique for quantitative determination of heat transfer coefficient and found that the results agreed well with the measurements taken with conventional techniques. Simonich and Moffat(1984) used liquid crystals to study heat transfer on a concavely curved turbulent boundary layer. They developed a technique for instantaneous heat transfer measurement to provide a clear picture of local surface heat transfer coefficient on concave surfaces such as the ones existing on turbine blades. Hippensteele et. al(1985) used liquid crystals to map the local heat transfer coefficients along the mid chord of a five times size turbine blade airfoil in a static cascade operated at room temperature over a range of Reynolds numbers. They compared these results with the analytical values of heat transfer coefficients obtained from the STAN5 boundary layer code. Their results indicated that the composite of liquid crystals and the heater element sheet bonded to a model turbine blade provides an accurate, quantitative, and continuous map of heat transfer coefficients on the blade surface.

Hippensteele et.al (1987) used liquid crystals for quantitative, high resolution heat transfer coefficients on a turbine airfoil, including turbulence and surface roughness effects. In 1988, the same authors made use of liquid crystals for heat transfer measurements on the end wall of a turbine passage. Jones and Hippensteele (1988) used liquid crystals for heat transfer coefficient maps applicable to compound curve surfaces in a transient wind tunnel. Akimo et. al (1989) used a set of sharp band optical filters to

draw isothermal lines with the aid of digital image processing technique (Black and White) that excludes human color sensation.

Hollingsworth et.al (1989) used a wide band liquid crystal on a flat plate along with a true color digital image processing technique to measure the temperature distribution on a specimen. from its color image. Baughn et. al (1989) used liquid crystals to measure the local heat transfer coefficients on a pin fin.

The above digital image processing techniques used the RGB signals for associating color to temperature. Camci et. al (1991) developed a hue capturing technique for quantitative interpretation of liquid crystal images. They performed their experiments on the bottom surface of square to rectangular transition duct. Their interpretation included the use of a linear hue versus temperature relation as an accurate measuring tool and a transient heat transfer model for the conversion of time accurate temperature information into heat transfer coefficient maps. Camci et.al (1992) used the HSI technique to discuss the effect of the strength of the illuminating source, the heat transfer surface, effect of orientation of the illuminating source with respect to the surface, crystal layer uniformity, and the repeatability of the process. In 1993, Camci et.al used the above technique for evaluating the convective heat transfer coefficient maps on complex surfaces, and concluded that the usage of a narrow band of liquid crystal provided accurate results with very low uncertainty values.

Wang et. al.(1993) used a new method for processing liquid crystal signals from transient heat transfer experiments. They used the entire intensity history recorded during an experiment to obtain an accurate measurement of surface heat transfer coefficient. Farina et.al (1994) developed the HSI technique in which the results from the liquid crystal images were not dependent on the light source. Praisner et.al (1997) have used liquid crystal for spatial heat transfer distribution in the end wall junctions of a turbine passage.

This above discussion details on the various applications of liquid crystals in the heat transfer field. The following section discusses the calibration and data measurement technique employed in Michigan State University for mapping heat transfer/temperature distribution technique on a flat surface.

Calibration

The response of the encapsulated liquid crystals can differ between nominally the same coating composition. In the experiments performed, a particular liquid crystal coating is always calibrated in a calibration facility which approximates the experimental conditions very closely.

A sketch of the Calibration facility is shown in Figure B1.

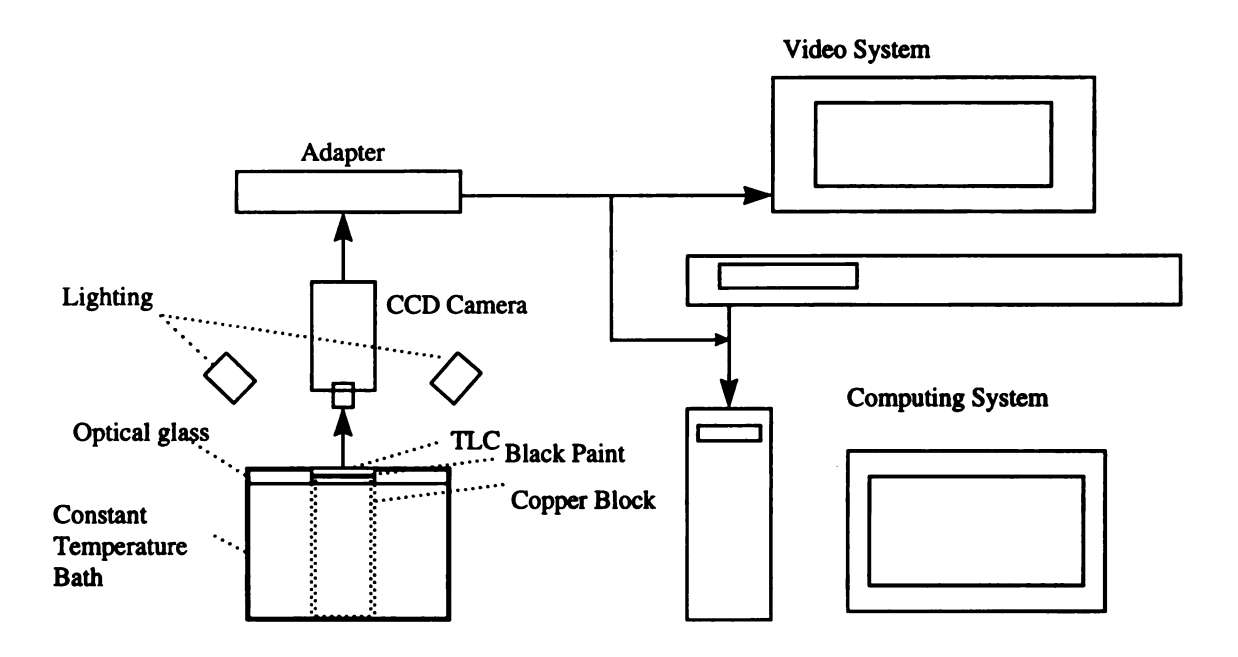


Figure B1. Calibration Facility of Liquid Crystals

Calibration is performed by coating the top of a copper block with a thin layer of liquid crystal coating over a thin layer of black paint coating. This block is 76.2mm square by 128.6mm high. The top is notched so that the area that the liquid crystals cover is slightly smaller than the rest of the block at only 63.5mm square. This layer of liquid crystals is checked with a micrometer to ensure that they are the same thickness as the layer on the test surface. The copper block is partially submerged in a constant temperature water bath which is insulated on the top by a layer of air trapped between the copper block and a flat plate of optical glass. The optical glass serves to insulate, to prevent glare, and to simulate experimental viewing conditions. The digital camera is set up at approximately the same angle with relation to the surface of the liquid crystals and lighting source as it is in the test section. A T-type thermocouple is flush mounted to side of the copper block at a distance of 12.8mm from the top surface. This thermocouple is used for determining the

temperature of the copper block during the calibration purpose. Care should be taken to insure that the temperature reading from the thermocouple matches with the constant temperature bath reading during the calibration process, which serves to act as a method for determining the insulation provided for the copper block.

Calibration is performed for the entire band of liquid crystals. Images are recorded every 0.5°C between the lower end and the higher end of the sensitive range of the liquid crystals. Once steady state is reached for a certain specified temperature, the liquid crystal image is grabbed using a Sony CCD Camera attached to a Matrox Marvel II frame grabber board fit into an IBM PC and saved into a file or the images can be recorded using a VCR and analyzed later. The Matrox Marvel II board is capable of grabbing 24 bit images at 30 frames per second, which is useful for both transient as well as steady state measurements. As soon as an image is grabbed, it is analyzed frame by frame using standard Image processing tools (MATLAB, in this case) at each of the temperatures to determine the average hue values corresponding to each temperature. These images have been analyzed both as 8 bit (256 colors) as well as 24 bit images (16 million colors).

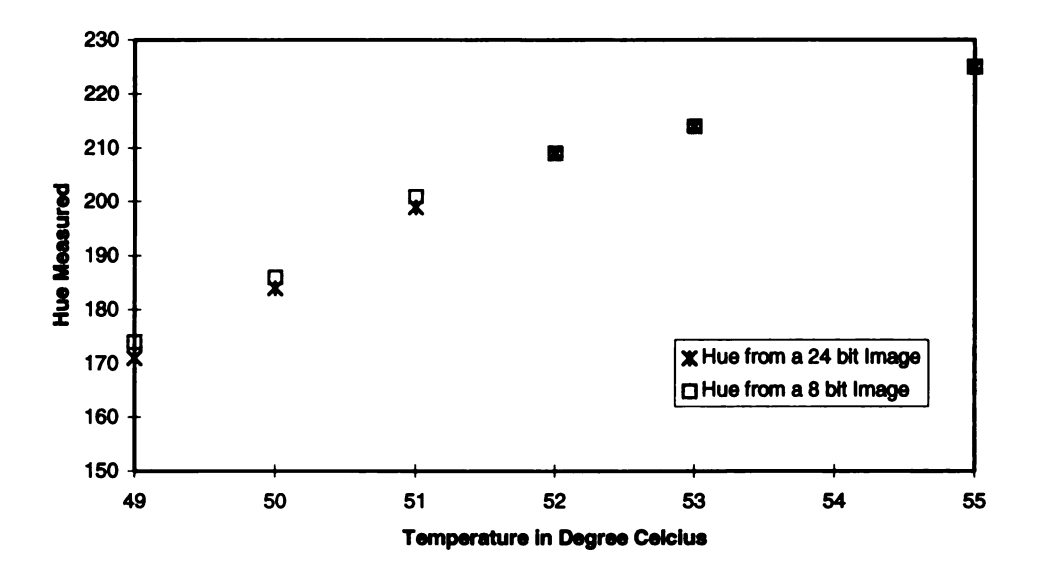
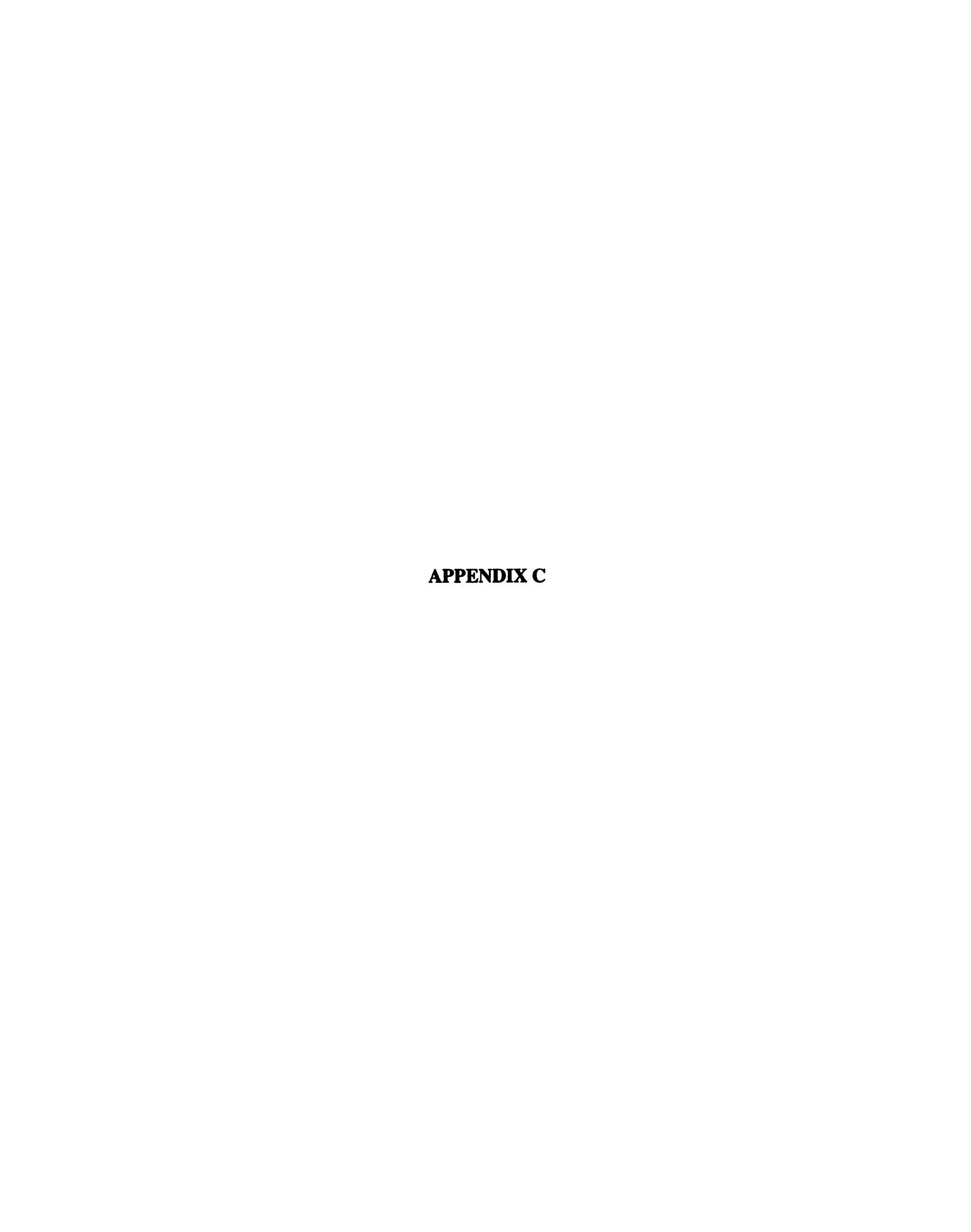


Figure B2. Comparison of 8 bit versus 24 bit values

Using the MATLAB toolbox, the grabbed images are converted into Red, Green and Blue (RGB) signals, pixel by pixel. These images have been analyzed both as 8 bit (256 colors) as well as 24 bit images (16 million colors) (Figure B2). Using standard conversion factors, these three signals are converted into hue, saturation and intensity values. The equations for conversion from RGB to HSI are as follows

To ease the process of collecting and analyzing the data, a program written using LABVIEW software provided a step by step procedure for the user to follow when calibrating and collecting data. LABVIEW served as a controlling software which called various subroutines which were capable of performing different tasks depending on the users desires. This program had the capability to calibrate liquid crystals as well as analyze data that had been collected. LABVIEW uses a MATLAB program to convert the

hue values found on the plate into temperature data using the calibration values that were generated prior to performing the experiment. A detailed report on the LABVIEW software is attached in APPENDIX C.

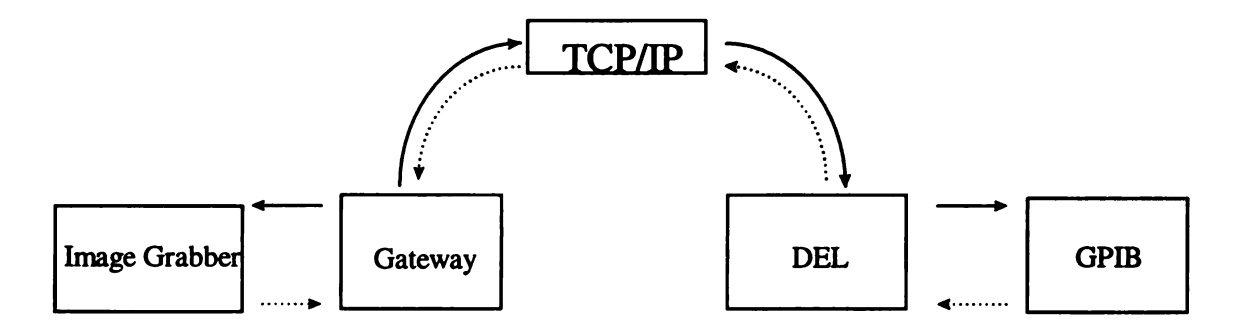


APPENDIX C

LABVIEW SOFTWARE REPORT

This software is written primarily for the image acquisition and analysis process for a liquid crystal thermal image. It links this with the temperature/pressure data acquisition done by the HP Data Acquisition system through the network, using LABVIEW.

The overall control flow for this entire process is shown in Figure C1. There are principally two computers, one(GATEWAY) for the image acquisition and analysis process using the image grabbing card and the other (DEL) for collecting thermocouple and pressure transducer data using the GPIB card, which is connected with the HP data Acquisition System. These two computers are linked by a transfer control protocol written in LABVIEW, so that the temperature/pressure data and the image data are collected simultaneously in the two different computers using the networking facility available. This entire process is done in real time. The overall control program for this entire process resides in the GATEWAY computer because the image processing (which takes up a lot of time) is done in this computer.



- indicates the trigger path sent from Computer I to the Grabber and also through the NetWork to Computer
- indicates the data path from Computer II, Image to Computer I

Figure C1. Overall System Design

As mentioned earlier, the gateway computer acts as the controller for this entire routine. When the experiment is run at steady state conditions, a button is pressed in the LABVIEW software which sends two signals simultaneously. One of them triggers the image acquisition process while the second one acquires the pressure and temperature data using the thermocouples and pressure sensors connected to the HP Data Acquisition System. As a recap, the image acquisition is done using the GATEWAY System, and the other parameters are acquired using the DEL System.

Having given a brief introduction about the overall control logic for the entire software, now we concentrate on the image acquisition and analysis part of the software. The flowchart for the image acquisition part is provided in Figure C2.

Initializing the Software

In order to start the software the user has to click on the LABVIEW icon. A list of sub directories are shown and the user has to choose the Liquid crystal program directory

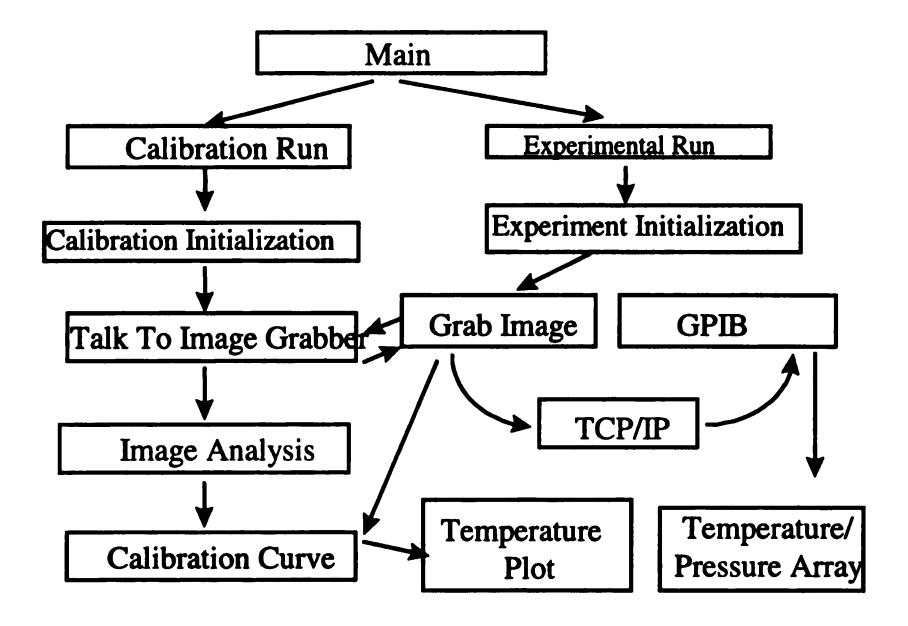


Figure C2. Flowchart of the control algorithm

folder (Make sure that this is shared with the other computer DEL). Once into this folder, there are a list of virtual instruments which would be used for this entire process. Choose the **Output Panel1.vi** by double clicking on it and this brings up the first screen in the

software. The Run button is activated in LABVIEW (the small => in the tool bar), and the RUN EXPERIMENT button is pressed. This brings up another window which gives the user an option of using either the calibration process or the experimental grabbing process. One of the options is used for calibrating the liquid crystals, and the other option is used for experimental testing.

Calibration

The calibration flow path is characterized by three sub programs. The first one is called calibration initialization.vi. This vi offers a list of checks that are to be taken care before going ahead with the calibration process. The user has to click on the rectangular buttons whenever he has completed the mentioned tasks. Once the user clicks the rectangular button, the circular indicator on the right side of that button changes color (from Green to Red) indicating that the particular step has been completed. Once the user has clicked all three rectangular buttons, the next subprogram calgrab.vi is initiated.

The calgrab vi performs the image grabbing process. The user has to specify the total number of images that he wishes to grab during the calibration process in the specified rectangular control box. Once he has specified the number, he has to press the ENTER button to register that value. After this, the user waits for steady state conditions to be reached for the first calibration point or temperature. As soon as steady state is reached, the user presses the GRAB button at the lower left hand corner of the screen. This triggers a signal to be sent to the image grabbing board and a frame of the image at that particular

temperature is brought up on the screen, and a dialog box asking for the filename under which the image is to be saved is brought up. (Note: The file is always saved on the D:\ drive. The file, at this point of time cannot be saved in any other directory or drive). The user has to type in an appropriate name in the filename box and hit the OK button. This will save that particular file under that name. Also there would be an update of the number of images that have been grabbed till that point of time in the indicator box on the right hand top corner of the screen. This process of pressing the GRAB button and saving the file is repeated for all the calibration points (i.e.,= to the total number of images). Once all the images have been grabbed the image analysis sub program called calib analy.vi is brought up. Before this is activated, there is message prompt which says that MATLAB would be loaded for the image analysis purposes, and that the user has to use the MATLAB program named cal (which stands for calibration) for this analysis purpose. The user has to pay careful attention to the instructions that are brought up at this point of time, because the user has to be careful while selecting the window within which the image analysis is to be performed.

In the image analysis sub program, MATLAB is started and the program written for analyzing the images is loaded by typing "cal" at the matlab prompt. After this, a few inputs as to the name of the image file, the number of pixels that need to be skipped while carrying out the image analysis routine, the window of the image file within which the averaging of the pixel values need to be done are chosen using the left and right mouse button. (The left mouse button is used to choose the upper left corner of the averaging area and the right mouse button is used for choosing the lower right hand corner of the

averaging area). After this the program averages the hue value between these two end points in the window. Once the processing of the image is done(indicated by the mouse pointer shape) the user closes the image window in MATLAB, and the temperature at which that particular image was recorded is given as an input to the program. This writes the hue value associated with the first image along with the corresponding temperature into a file called calbfile.xls. The program prompts for the second image file, and the above process is repeated until all the calibration images have been analyzed. Once all the images are analyzed, the button which says 'DONE WITH MATLAB' is flipped to the YES position. This initiates a curve fitting routine (a second order polynomial best fit), and the calibration curve between the temperature and the hue value is thus generated. The calibration equation is saved under a file called CALEQU.TXT and the coefficients of the calibration equation is saved in a file called CALCOEFF.TXT. These two files are saved in the 'D:\' drive and they are used for the experimental run routine. A typical calibration curve is shown in Figure C3. And the associated calibration equation of the best fit second order line is as follows

$$T_{avg} = 0.000281 \cdot Hue^2 + 0.00657 \cdot Hue + 29.079284$$
 (1)

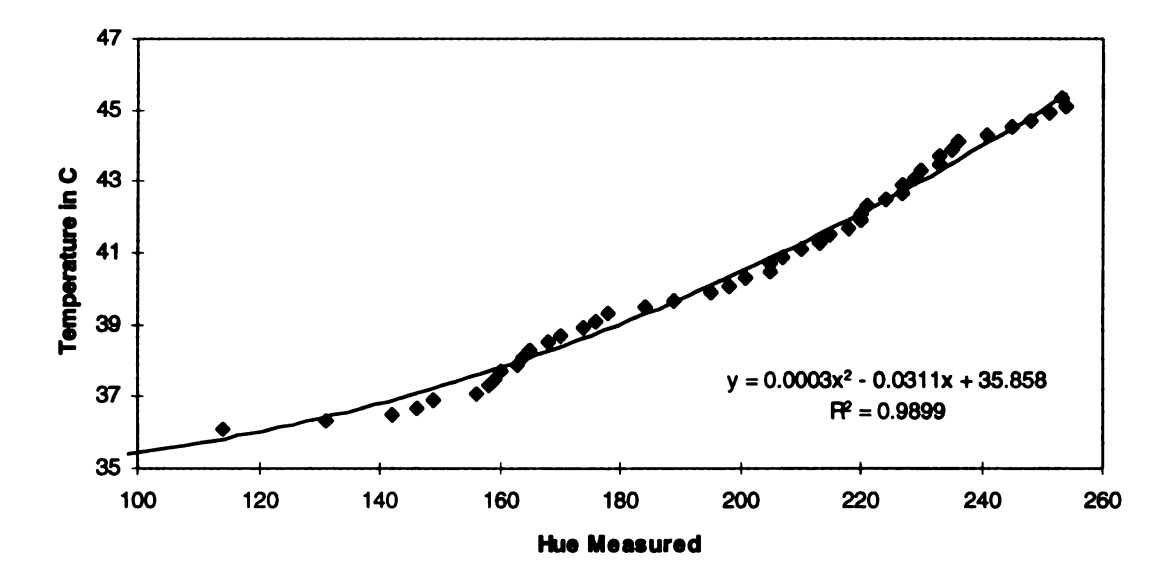


Figure C3. Second Order Polynomial Fit for Hue versus Temperature.

This calibration equation is then used for getting the surface temperature distribution of the image grabbed under steady state when the actual experiment is run.

EXPERIMENTAL RUN

The data for the experiment is collected using a very similar setup as was used during the calibration phase. This flow path is activated by using the experimental run option instead of the calibration run option. There are a set of initial conditions that are tested for the experimental setup, which is done using the experimental initialization.vi. Once all the conditions are tested, the experimental grabbing.vi is activated. This vi grabs the experimental image, and the image is saved in the D:\ drive (Note: The location of these files can't be altered, and they have to reside in the D:\ drive). The salient feature of this vi is that when the GRAB button is pressed, a trigger is sent to the image grabbing card to

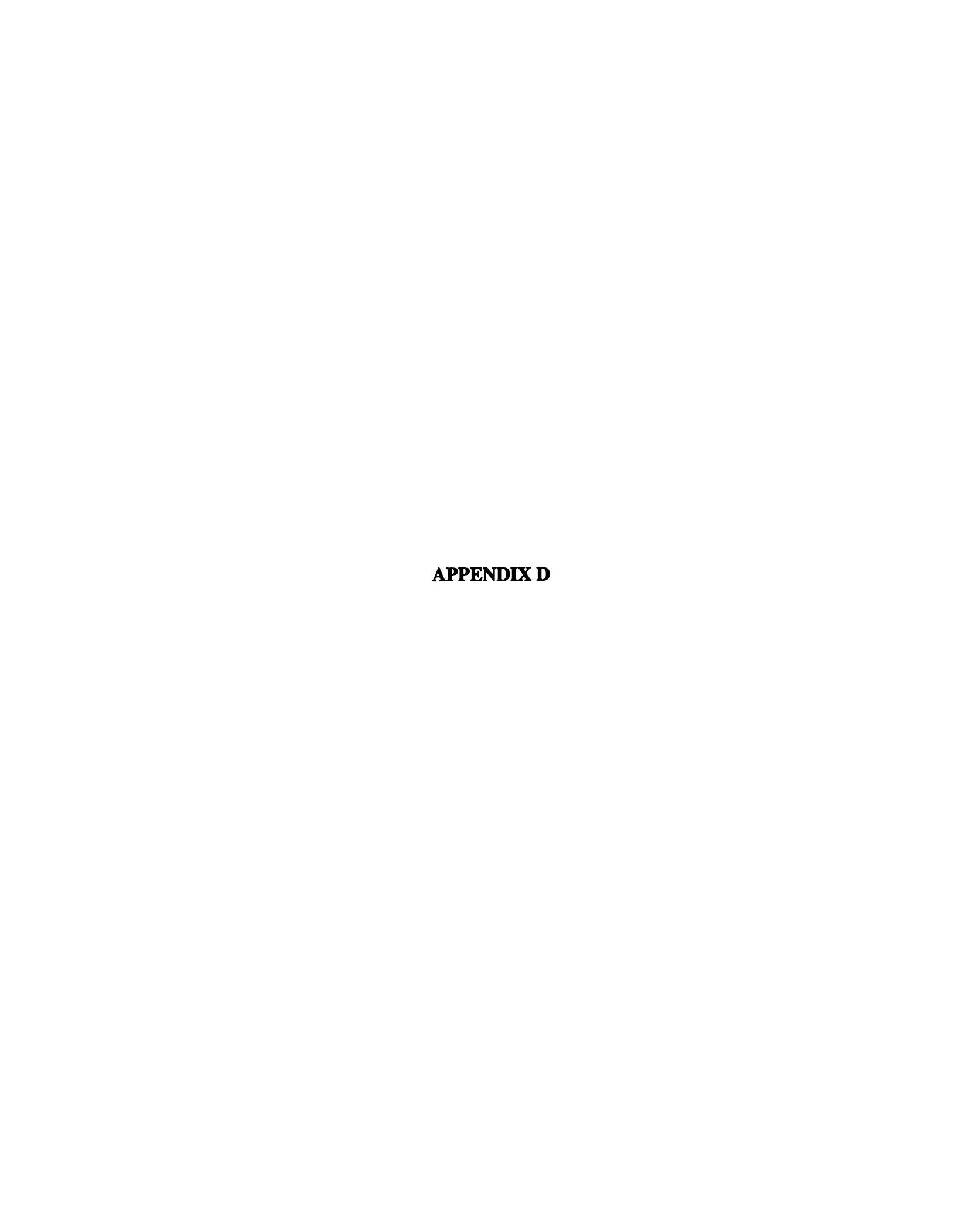
grab the image, and at the same instant another trigger is generated which travels across the network through the transfer call protocol (Figure C1), and the pressure and thermocouple data of the flow is recorded in the DEL computer. Once these sets of data have been collected, the image analysis is done using MATLAB as before. Before executing the experimental analysis program, another program called dimes is activated.

The dimens program is used for converting the pixel locations into 'x' and 'y' coordiante values in terms of meters. By typing dimens at the MATLAB prompt, this program is executed and a bunch of inputs such as the name of the image file, the length of the plate along the flow direction and across the flow direction and the extremities of the plate pixel locations(by mouse clicks) are given. These inputs initiate the calculation of the length of each pixels in both the 'x' and 'y' directions. These values are stored in dimensi.txt

After that the image window is closed and the image analysis program is activated. To activate the experimental image analysis program, the program exper is executed, which asks for the following inputs namely, the name of the image file and the window within which the image is to be analyzed. The user also has to specify the number of pixel that needs to be skipped for the analysis. (Note: The number of pixels to be skipped determines the rate at which the results of the analysis are given. i.e, the lower this number, the longer it takes for the analysis to complete. The default is set to 10).

These input specifications allows the hue values for the image to be computed as before, and they are converted into corresponding temperatures using the calibration equation. This entire process is automated. Since the conversion from the image to RGB values to HUE values to Temperature values involves lot of computation, the process is not dynamic, though the data part is dynamic. A possible way of altering this could be by using the board itself to access the data and convert it into hue values instead of using MATLAB to convert the image into RGB values, which is not currently being done. Instead the entire process is done by the software. This controlling by the hardware is required, if one were to run transient analysis on the liquid crystal data.

Once the analysis is done, the MATLAB window closes automatically, and the user can make use of the 'DONE WITH MATLAB' button. Switching this button towards the YES direction loads all the data into the table, and there are a couple of prompts which ask whether you want to replace the existing files. The user takes an appropriate action by saying REPLACE, and then he has to click the DONE button. This would take the control to the main window, and when the user clicks on PLOT DATA button, the results which are originally in a file which has three columns (Name of the file is TEMPVAL.XLS, and this is in the D:\ drive) is converted into a rectangular matrix depending on the number of pixels in the X and Y directions, and this resultant file is stored in the file TEMP_MAT.xls.



APPENDIX D

Instructions for the MATLAB based Liquid Crystal program

Calibration:

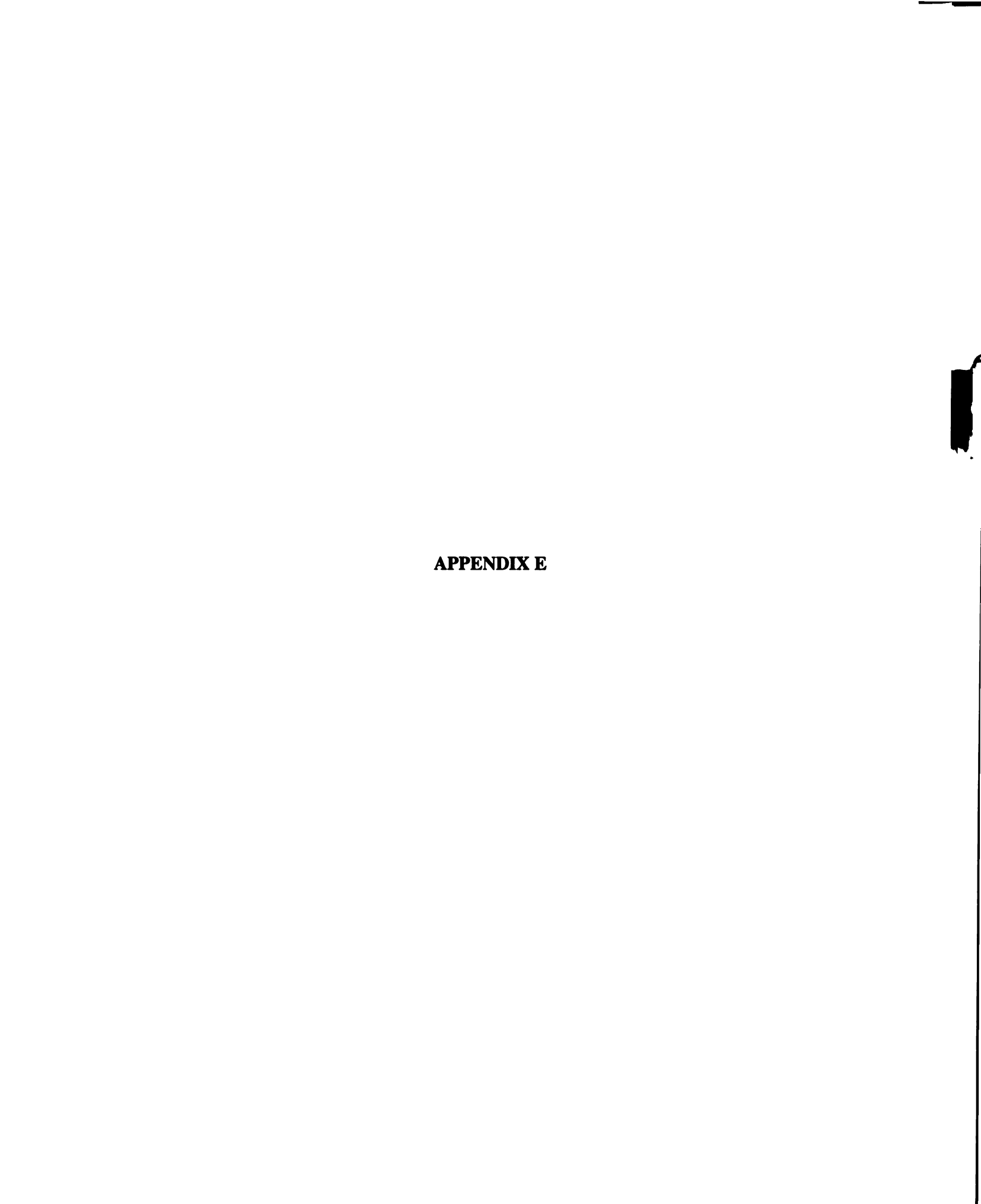
- (i) Assume that the calibration setup is ready.
- (ii) Using the temperature controller set the first temperature for calibration
- (iii) allow system to reach steady state
- (iv) using MyComputer, go to D:\ double click the grab.exe to grab the first image, and give an appropriate name for the file. (for testing purposes dy existing files namely ME491290, ME491295 etc.,)
- (v) Once you have grabbed all the images, go to *MyComputer*, open up the file *D:WoFrames.xls* and change the first number to indicate the number of images that you have grabbed and save the file back in the same place using Save As.
- (vi) Now open MATLAB using Start->Programs->MATLAB for windows-> MATLAB
- (vii) Type in *cal* at the matlab prompt and follow instructions. Once you have analyzed all the images, the results of the calibration is stored in a file *D:\calbfile.xls*. Close MATLAB.
- (viii) Open up the *D:\calbfile.xls* file and plot Temperature versus Hue and not Hue versus Temperature using scatter plot. To insert a trendline, first double click the chart, and then single click anyone of the data points. Now go to *INSERT* ->

Trendline menu option, fit a second order polynomial, and using the *OPTIONS* within that window, choose an option so that the equation of the polynomial is shown in the figure. Make a note of this polynomial. After this open D:\CALCOEFF.xls, and enter the coefficients of the calibration equation into this file in the same order as present in the equation (i.e., 2nd order first, 1st order and the constant).

Experimental Run

- (i) Assume that the experimental setup is ready.
- (ii) Wait for steady state to be reached.
- (iii) Using D:\grab.exe, grab the image and save it in an appropriate file name.
- (iv) Now open MATLAB using Start->Programs->MATLAB for windows-> MATLAB
- (v) Type in *dimens* at the MATLAB prompt. This program is used to convert the pixel coordinates into the xy coorinates positions in terms of meters and follow the instructions. The output of this file is stored in *D:\Dimensi.txt*, which contains information about the pixels lengths in terms of meters. After this close the figure window.
- (vi) Now type in *exper* at the MATLAB prompt, and follow the instructions to analyze the image. Once you have analyzed the image, MATLAB would automatically close, and the output of the analysis is stored in files namely *D:\Hu_valpi.xls*, and *D:\Hu_value.xls*

- (vii) The above two files contains only the Hue values in each pixel location in terms of pixel coordinates and xy coordinates (meters) respectively. Both the files are 3 column files, and the third column is where the Hue values are stored.
- (viii) Now in order to transform the file from a three column hue values file to a three column temperature file and then to a rectangular matrix, you have to rerun MATLAB. Open MATLAB as before, and type in *transfrm* at the *MATLAB* prompt and this program automatically creates two output files namely TEMP_VAL.xls and temp_mat.xls. For more information about these files refer to APPENDIX E.



APPENDIX E

List of files and the information stored in them

The names of the files used in the program

LABVIEW files

Output panel1.vi MAIN1.vi calibration initialization 1.vi cal grab.vi matlab analysis calibration.vi

experimental initialization 1.vi EXPERIMENTAL GRABBING1.vi matlab analysis 1.vi

globalctl.gbl global2.gbl global3.gbl

List of MATLAB program files

cal.m exper.m dimens.m transfrm.m bmpread4.m

List of DATA files

Dimensi.txt
Calbfile.xls
CALCOEFF.xls
Calequ.txt
NoFrames.xls
Hu_valpi.xls
Hu_value.xls
TEMP_Val.XLS
temp_mat.xls

Output Panel1.vi

The front panel in this LABVIEW program is where the entire control algorithm starts for the liquid crystal calibration as well as the experiment. The are three blocks in this front panel. One block which can list the temperature and pressure data, of the flow, that is got from the DAQ. One chart which gives the surface temperature distribution from the liquid crystal image, when the PLOT DATA button is pressed. And the third button which causes the entire sequence of this program to execute. The PLOT DATA button is pressed at the end of the entire sequence of the experimental run. This results in the data that is stored in three columns in the 'TEMP_VAL.xls' to be converted into a rectangular matrix and stores the rectangular temperature matrix into a file called 'temp_mat.xls'.

MAIN1. Vi

The front panel of this LABVIEW program contains two things namely CALIBRATION RUN and EXPERIMENTAL RUN, which are self explanatory. The user clicks on either one of these buttons depending on what needs to be done.

CALIBRATION INTIALIZATION.VI

This part of the LABVIEW front panel has a bunch of controls and indicators. The controls are the one's on the left hand side of the panel, and the indicators are on the right hand side of this panel. Presently all these controls have to be manually done. The idea behind having this initialization process is to aid any person who uses the liquid crystals

to take appropriate care to go through all these steps before commencing the calibration process. When the user clicks on the controls the indicator against these controls automatically change their colors from GREEN to RED. Also these controls can be used to activate motors (if the proper instruments are made available, instead of manual operations, as is currently being done) to take necessary actions.

CAL GRAB.VI

This program is used for grabbing the images while calibrating the liquid crystals. The user has to specify the number of images that s/he wants to grab (which is directly proportional to the number of temperatures that s/he wants to calibrate the liquid crystals at). The value that the user specifies here is stored in the 'NoFrames.xls' file. Once specified, the user waits for steady state to reach for the first set temperature (the user has to watch the TV screen for this purpose). Once s/he is satisfied with the steady state condition, the image is grabbed by clicking on the GRAB button. This would allow the image to be saved in a file that is stored in the REMOVABLE DISK DRIVE (D:\). Note that if the user runs into any problems while grabbing the images s/he can restart the grabbing process, but the number of images to be grabbed has to be modified accordingly when it is run the second time. Also once all the images have been grabbed, before running the MATLAB program 'cal', the user has to open the file Noframes.xls and check if the first number indicates the total number of images that have been grabbed during the entire calibration process.

MATLAB ANALYSIS CALIBRATION.VI

The front panel of this program has three blocks, one to check whether the MATLAB part of the analysis is completed, the second to display the hue values corresponding to each temperature, and the third block is to displace the calibration equation, which relates the Temperature to the HUE values by means of a second order polynomial. The output files created out of this program are

- (i) 'calbfile.xls', where the hue values corresponding to each temperature is stored
- (ii) 'calequ.txt', where the calibration equation is stored
- (iii) 'calcoeff.txt', where the coefficients of the calibration equation is stored.

All the above files are stored in the REMOVABLE DISK DRIVE (D:\).

EXPERIMENT INITIALIZATION 1.VI

This part of the LABVIEW front panel, similar to the CALIBRATION INITIALIZATION VI, has a bunch of controls and indicators. The controls are the one's on the left hand side of the panel, and the indicators are on the right hand side of this panel. Presently all these controls have to be manually done. The idea behind having this initialization process is to aid any person who uses the liquid crystals to take appropriate care to go through all these steps before commencing the experimental run process. When the user clicks on the controls the indicator against these controls automatically change

their colors from GREEN to RED. Also these controls can be used to activate motors (if the proper instruments are made available, instead of manual operations, as is currently being done) to take necessary actions.

EXPERIMENTAL GRABBING 1.VI

This front panel has just one button, which is used for grabbing the steady state image when the experiment is run. Once s/he is satisfied with the steady state condition, the image is grabbed by clicking on the GRAB button. This would allow the image to be saved in a file that is stored in the REMOVABLE DISK DRIVE (D:\).

MATLAB ANALYSIS 1.VI

The front panel of this program has three blocks, one to check whether the MATLAB part of the analysis is completed, the second to display the hue values corresponding to each temperature, and the third block is to displace the calibration equation, which relates the Temperature to the HUE values by means of a second order polynomial. The output files created out of this program are

- (i) 'Hu_ValPi.xls', which saves the pixel location and the corresponding hue values in a three column matrix.
- (ii) 'Hu_Value.xls', which saves the 'x' and 'y' coordinates and the corresponding hue values in a three column matrix.
- (iii) 'TEMP_VAL.XLS', which saves the 'x' and 'y' coordinates and the corresponding temperature values in a three column matrix.

cal.m

This is a MATLAB file which is used while the calibration is done. This program analyzes every image, and computes the average hue value within the specified window. The hue value is matched with the corresponding temperature and the results of this is placed in a file called Calbfile.xls. The inputs that this program needs are the file name of the image to be anlayzed, the window within which the hue values have to be computed, the number of the pixels that need to be skipped during this calculation procedure, and the temperature at which the calibration is done. Depending on the number of the images that have been grabbed (this value is stored in NoFrames.xls), the above process has to be repeated that many times.

dimens.m

This is again a MATLAB file which is used in converting the pixel locations into x and y coordinate locations. This file is executed before exper.m. The basic function of this is to create an output file with information about how much each pixel length corresponds to in terms of distance in meters. For this purpose, the user has to give inputs like the distance of the plate(that is encompassed in the view) along the flow as well as across the flow. The user needs to specify the name of the image file (NOTE: The image of the plate has to be at aligned perfectly with the 'x' and 'y' axis, and cannot be at an angle.), and using the mouse has to pick the pixels at the extremes of the plate location using the left and right mouse buttons respectively. The output of this program is stored in dimensi.txt and is made use of by exper.m file

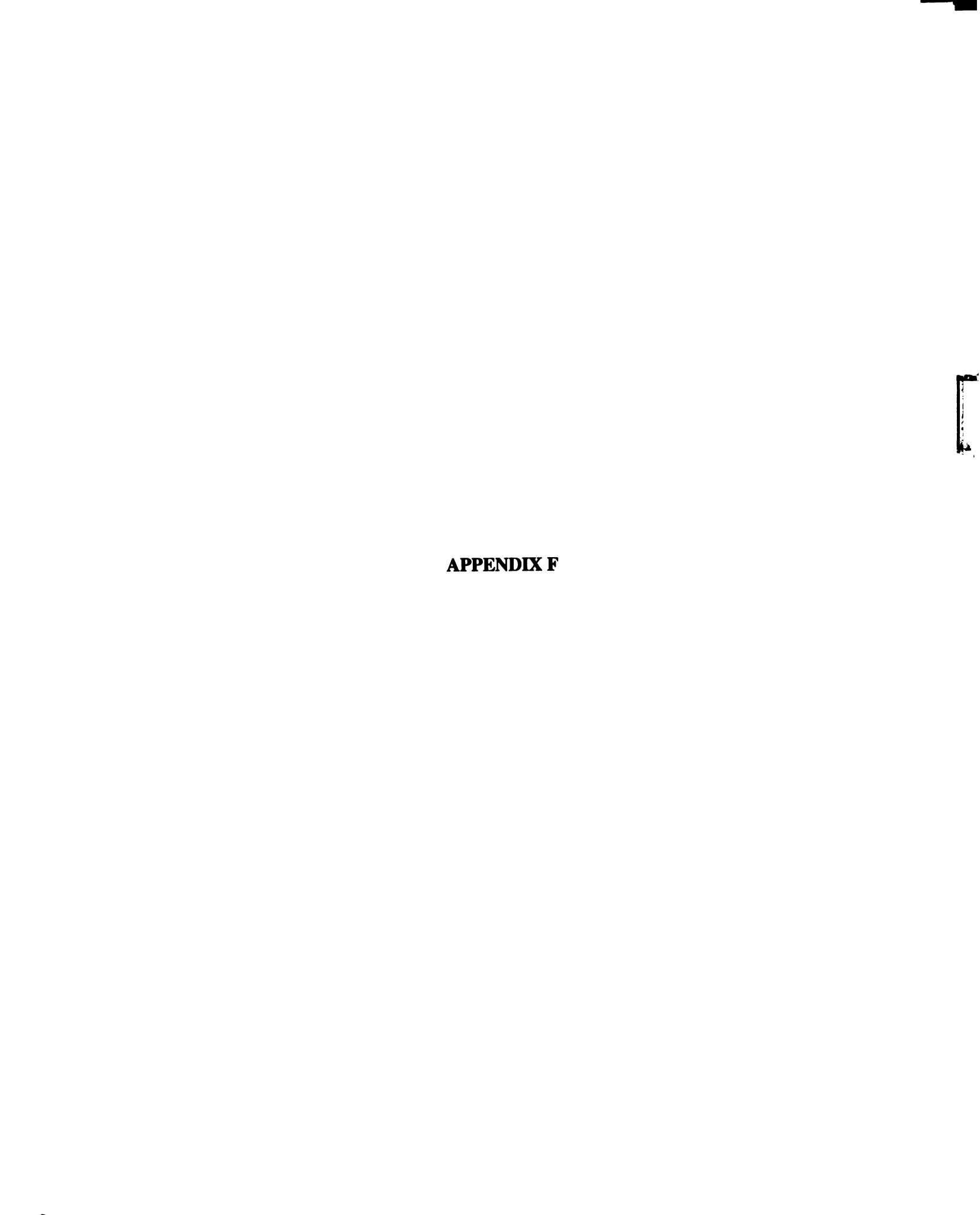
exper.m

This MATLAB file is used for analyzing the experimental image, and converts the pixel image into hue values. The inputs that this program requires are the file name of the image, number of pixels to skip and the output is a three column matrix which is stored in two files namely, Hu_valpi.xls and Hu_value.xls. The first two columns in Hu_valpi.xls are the 'x' and 'y' pixel locations, while the first two columns in Hu_value.xls are the 'x' and 'y' coordinates in terms of meters. The third column in both these files is the hue at that particular location.

transfrm.m

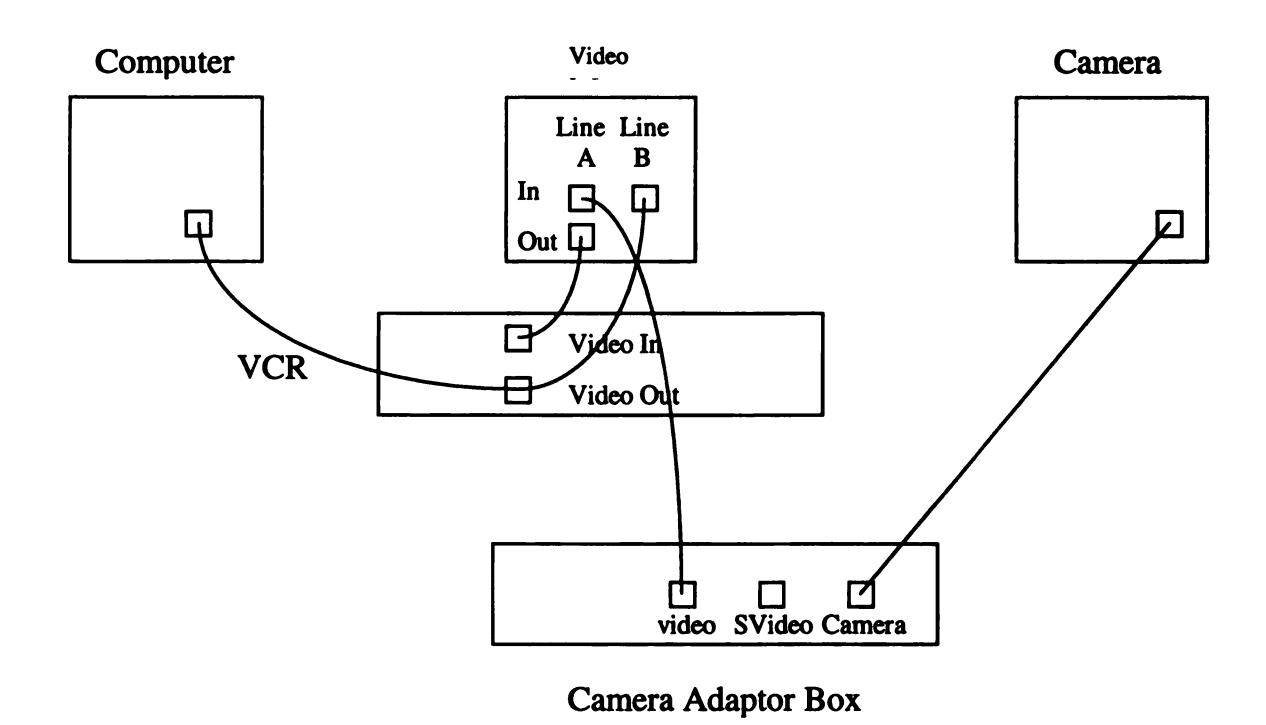
This MATLAB file is used for the standalone program(Appendix D) only. This is used to convert the three column matrix got out of exper.m into a rectangular matrix and stores the output temperature matrix in a file D:\temp_mat.xls.

If LABVIEW were not being used for the image anlaysis process, then the user needs to follow the instructions provided in Appendix D to go through the liquid crystal analysis process.



Appendix F

Image Acquisition Experiment Setup



Note: The connection from the video out of the VIDEO to the computer must be connected through the Video A cable.

REFERENCES

REFERENCES

Abe, T., et. al., "Cooling characteristics of film cooled turbine blades", ASME 84-GT-73.

Abuaf, N., et.al., "Convection thermography", Technical Information Series, General Electric, September 1985, Report No. 85CRD168.

Akino, N., et. al., "Improved liquid crystal thermometry excluding human color sensation", Journal of Heat Transfer, Transactions of ASME, Vol. 111, May 1989, pp.558-565.

Akino, N., et. al., "Liquid Crystal thermometry based on automatic color evaluation and applications to measure turbulent heat transfer", Transport Phenomena in turbulent flows, 1988.

Arseniev, L.V., et. al., "Combined Cycle plant based on high temperature steam cooled gas turbine", 1991 ASME Cogen-Turbo, IGTI-Vol. 6, pp. 31-37.

Baughn, J.W., et.al, "Local Heat Transfer measurements using an electrically heated thin gold coated plastic sheet", Journal of Heat Transfer, Nov. 1985, vol.107, pp. 953-959

Baughn, J.W., et.al., "A comparison of the transient and heated coating methods for measurement of local heat transfer coefficients on a pin fin", Journal of Heat transfer, Nov 1989, Vol. 111, pp.877-881

Baughn, J.W., et.al., "Improvements in a new technique for measuring and mapping heat transfer coefficients", American Institute of Physics, Rev. Sci. Instrum. 57(4), April 1986, pp.650-654.

Bejan, A., Convective Heat transfer, John Wiley & Sons Inc, New York, 1995, pp. 39-47.

Bettagli, N., "Blade cooling improvements in combined cycle power plants", Proceedings of ASME Cogen-Turbo Power conference, 1995, 95-CTP-91.

Boyle, R.J., "Heat transfer in serpentine passages with turbulence promoters", 1984, ASME paper 84-HT-24.

Camci, C., et.al., "A new hue capturing technique for quantitative interpretation of liquid crystal images used in convective heat transfer studies", Journal of turbomachinery, Oct. 992, Vol. 114, pp. 765-775.

Camci, C., et.al., "Convection heat transfer at the curved bottom surface of a square to rectangular transition duct using a new hue capturing based liquid crystal technique", Fundamental experimental measurements in heat transfer, HTD-Vol. 179, ASME 1991, pp. 7-22.

Camci, C., et.al., "Evaluation of a hue based transient liquid crystal method for high resolution mapping of convective heat transfer on curved surfaces", Journal of Heat transfer, May 1993, vol. 115, pp. 311-318.

Churchill, S. W. and Ozoe, H., 1973, "Correlations for Laminar forced Convection with Uniform Heating in Flow over a Plate and in Developing and Fully developed Flow in a Tube", Journal of Heat Transfer, Vol. 95, pp. 78 - 84.

Churchill, S.W., "A comprehensive correlating equation for Laminar, Assisting, forced and free convection", AIChE Journal, Vol.23, 1977, pp. 10-16.

Chyu, M.K., "Regional Heat transfer in two pass and three pass passages with 180 deg sharp turns", Journal of Heat transfer, 1991, Vol. 113, pp. 63-70.

Coleman, H.C., et. al., "The accelerated fully rough turbulent boundary layer", Jn. of fluid mechanics, 1977, pp. 507-528.

Conklin, G.E., Han, J.C., and Jenkins, P.E., "Film Cooling with Steam injection through three staggered rows of inclined holes over a straight airfoil", ASME Paper No. 83-GT-30, 1983.

Cook, B. D., et.al., "Mapping ultrasonic fields with cholesteric liquid crystals", Ultrasonics, Apr. 1971, pp. 101-102.

Cooper, T.E., and Groff, J.P., "Thermal mapping via liquid crystals of the temperature field near a heated surgical probe," Journal of heat transfer, Trans. ASME, series C, vol. 95, No.2, 1973, pp. 250-256.

Cooper, T.E., and Petrovic, W.K., "An experimental investigation of the temperature field produced by a cryosurgical cannula," Journal of heat transfer, trans ASME, Series C, Vol. 96, Bo.#, Aug. 1974, pp.415-420.

Cooper, T.E., et. al., "Liquid crystal Thermography and its application to the study of convective heat transfer", Journal of heat transfer, 1975,pp. 442-450.

Crissey, J.T., et. al., "A new technique for determination of the skin temperature patterns", Journal of Investigative Dermatology, Vol.42, No.2, Aug 1964, p.89.

Crissey, J.T., et. al., "Cutaneous thermography with liquid crystals", Journal of Investigative Dermatology, Vol.45, No.5, Nov. 1965, p.329.

Dini., S., et.al., "Use of liquid crystal for local heat transfer coefficient measurement around 180° bend", Fundamentals of forced convection heat transfer, HTD-Vol. 210, ASME 1992, pp. 107-114.

Dowden, W.A., "Cholesteric Liquid Crystals: A review of developments and applications," Non-Destructive testing, Vol.1, No.2, Nov. 1967, pp.99-102.

Dring, R.P., et. al., "An experimental investigation of film cooling on a turbine rotor", Jn. of Eng. For Power, Vol. 102, 1980, pp. 81-87.

Eckert, E.R.G., 'Transpiration and Film cooling', Mass transfer, pp.195-210.

Eckert, E.R.G., and Livinghood, J.N.B., "Comparison of effectiveness of convection, transpiration and film cooling methods with air as a coolant", Report 1182, National Advisory Committee for Aeronautics, 1954.

Ekkad, S.V., and Han, J.C., "Flat plate film cooling and heat transfer using a transient liquid crystal technique", ASME/JSME Thermal Engineering Conference, Vol. 3, 1995, pp. 445-452.

Ennulat, R.D., and Fergason, J.L., "Thermal Radiography utilizing liquid crystals," Molecular crystals and Liquid crystals, Vol. 13, 1971, pp.149-164.

Farina, D.J., et. al., "Illuminant invariant calibration of thermochromic liquid crystals", Experimental thermal and fluid science 1994, Vol. 9, pp. 1-12.

Florschuetz, L.W., et. al., "Streamwise flow and heat transfer distributions for jet array impingement with crossflow", ASME 81-GT-77.

Florschuetz, L.W., et. al., "Periodic streamwise variations of heat transfer coefficients for inline and staggered arrays of circular jets with crossflows of spent air", Journal of heat transfer, 1980, Vol. 102, pp. 132-137.

Gillespie, D.R.H., et. al., "Detailed measurements of local heat transfer coefficient in the entrance to normal and inclined film cooling holes", Transactions of ASME, International Gas Turbine and AeroEngine Congress and Exposition, June 13-16,1994.

Goldstein, R.J., "Film cooling", Advances in heat transfer, Academic Press, New York, 1971, pp.7-321.

Hay, N., et.al., "Effects of cooling films on the heat transfer coefficient on a flat plate with zero mainstream pressure gradient", Journal of Engineering for Gas turbines and Power, Vol. 107, 1985, pp. 105-110.

Healzer, J.M., et. al., "Experimental heat transfer behavior of a turbulent boundary layer on a rough surface with blowing", Jn. Of Heat transfer, Vol. 100, 1978, pp. 134-142.

Hempel, H., et.al., "Full coverage film cooled balding in high temperature gas turbines: Cooling effectiveness, profile loss, and thermal efficiency". Journal of engineering for Power, 1980, pp. 957-963.

Hennecke, D.K., Turbine Blade cooling in Aero Engines- Some New results, future trends, and research requirements, pp. 1-15

Hippensteele, S.A., and Poinsatte, P.E., "Transient liquid crystal technique used to produce high resolution convective heat transfer coefficient maps", NASA Technical Memorandum 106083, Aug 1993.

Hippensteele, S.A., and Russell, L.M., "High resolution liquid crystal heat transfer measurements on the end wall of a turbine passage with variations in Reynolds number", NASA Technical Memorandum 100827, July, 1988.

Hippensteele, S.A., et.al., "Evaluation of a method for heat transfer measurements and thermal visualization using a composite of heater element and liquid crystals", Journal of Heat Transfer, vol.105, 1981, pp.184-189.

Hippensteele, S.A., et.al., "Local Heat transfer measurements on a large scale model turbine blade airfoil using a composite of heater element and liquid crystals", NASA Technical Memorandum 86900.

Hippensteele, S.A., et.al., "Use of a liquid crystal, heater element composite for quantitative, high resolution heat transfer coefficients on a turbine airfoil, including turbulence and surface roughness effects, NASA Technical Memorandum 87355, May 1987.

Hollingsworth, D.K., et.al., "Measurements of temperature and heat transfer coefficient distributions in a complex flow using liquid crystal thermography and true color image processing", Collected papers in Heat Transfer, Heat Transfer Division, 1989.

Hollworth, B.R., et.al., "Arrays of impinging jets with spent fluid removal through vent holes on the target surface. Part 2: local heat transfer", Journal of Engineering for Power, 1983, Vol. 105, pp. 393-402.

Ikeguchi, T., and Kawaike, K., "Effects of closed circuit gas turbine cooling systems on combined cycle performance", Proceedings of the ASME Joint International Power Generation conference, 1994, 94-JPGC-GT-8.

Ireland, P.T., et. al., "Liquid Crystal Heat transfer Measurements", Measurement Techniques, Von Karman Institute for fluid Dynamics, 1992-1993 Lecture series.

Ito, S., et. al., "Film cooling of gas turbine blade", Jn. Eng., for Power, vol. 100, 1978, pp. 476-481.

Je-Chin Han, "Turbine blade cooling", Heat Transfer in Thermal Systems Seminar-Phase II, Jan13-14,1986, pp.157-166.

Jones, T.V., "High resolution heat transfer coefficient maps applicable to compound curve surfaces using liquid crystals in a transient wind tunnel", NASA technical Memorandum 89855.

Katz, R.G., and Cooper, T.E., "Liquid Crystal Display of the temperature fields produced by radio frequency emitting electrodes," 26th ACEMB, conf. Proceed, Sept. 30-Oct. 4, 1973, p.257.

Kays, W.M., Convective Heat and Mass Transfer, McGraw-Hill, pp. 78-85.

Kikkawa, S., and Senda, M., "Transpiration cooling using air as a coolant", Trans. JSME 57 (542), 1991, 3531-3536.

Klein, D.J., "Liquid Crystals in Aerodynamic testing," Astronautics and Aeronautics, Vol.6, No.7, 1968, pp.70-73.

Larson, E.D., and Williams, R.H., "Steam Injected gas turbines", Journal of Engineering for Gas turbines and Power, 1987, pp. 55-63.

Maple. R.D., "Utilization of temperature sensitive liquid crystals for thermal analysis and an application to transducer investigations", Naval Underwater systems center TR 4235, May20, 1972.

Mayle, R.E., "Multihole cooling film Effectiveness and heat transfer", Jn. of Heat transfer, Vol. 97, 1975, pp.534.

Metzger, D.E., "Cooling techniques for gas turbine air foils - A survey", AGARD, 1985.

Metzger, D.E., et. al., "Effectiveness and heat transfer with full coverage film cooling", Jn. of Eng. For Power, 1973, pp. 180.

Metzger, D.E., et.al., "Heat transfer with film coolign near non tangential injection slots", Jn. of Eng. For Power, 1968, pp. 157-163.

Moffat, R.J., "Describing the uncertainties in experimental results", Experimental thermal and Fluid science, 1988, pp.3-17.

Moffat, R.J., "Turbine Blade cooling", Heat transfer and fluid flow in rotating machinery, 1987.

Moffat, R.J., and Kays, W.M., "The turbulent boundary layer on a porous plate: Experimental heat transfer with uniform blowing and sucking", Int. Jn. Of Heat and Mass transfer, Vol. 11, 1986, pp. 1547-1566.

Mori, Y., et.al., "Convective heat transfer in a rotating radial circular pipe", Int. J. of Heat and Mass Transfer, 14: 1807-1824, 1971.

Murthy, J.Y., and Chyu, M.K., "A numerical study of laminar flow and heat transfer in a channel with a 180 deg bend", 1987, ASME Paper 87-HT-7,

Orlando, A.F., et. al., "Heat transfer in turbulent flows under mild and strong adverse pressure gradient conditions for an arbitrary variation of the wall temperature", Proc. Of the 24th heat Transfer and Fluid Mechanics, Corvallis, Jun 1974.

Pimenta, M.M., et.al., "The structure of a boundary layer on a rough wall with blowing and heat transfer", Jn. Of Heat Transfer, Vol., 101, 1979, pp. 193-198.

Praisner, T.J., et. al., "Spatial temporal turbulent flow field and heat transfer behavior in end-wall junctions", Int. J. Heat and Fluid flow, 1997, pp. 142-151.

Radd, T., and Myer, J.E., "Nucleation studies in pool boiling on thin plates with liquid crystals," AIChe Journal, Vol. 5,1971, pp. 1260-1261.

Rice, I.G., "Steam Cooled Gas Turbine casings, struts, and disks in a Reheat Gas turbine combined cycle: Part I- Compressor and Combustor", Transactions of ASME, Journal of Engineering for Power, Vol. 105, 1983, pp. 844-850.

Rice, I.G., "Steam Cooled Gas Turbine casings, struts, and disks in a Reheat Gas turbine combined cycle: Part II- Gas generator turbine and Power Turbine", Transactions of ASME, Journal of Engineering for Power, Vol. 105, 1983, pp. 851-858

Rice, I.G., "The combined reheat gas turbine/steam turbine cycle, Part I- A critical analysis of the combined reheat gas turbine/Steam turbine cycle", ASME journal of Engineering for Power, Jan 1980.

Rice, I.G., "The combined reheat gas turbine/steam turbine cycle, Part II- THE LM 5000 Gas generator applied to the combined reheat gas turbine/steam turbine cycle", ASME journal of Engineering for Power, Jan 1980.

Rice, I.G., "The reheat gas turbine with steam blade cooling- A means of increasing reheat pressure, output and combined cycle efficiency", ASME journal of Engineering for Power, Jan 1982.

Rice, I.G., and Jenkins, P.E., "Comparison of the HTTT reheat gas turbine combined cycle with the HTTT Nonreheat gas turbine combined cycle", ASME Journal of Engineering for Power, Jan 1982.

Russell, L.M., et.al., "Measurements and Computational Analysis of Heat Transfer and Flow in a Simulated Turbine Blade Internal Cooling Passage", 29th Joint Propulsion Conference and Exhibit, AIAA-93-1797.

Sasaki, M., et. al., "Film Cooling effectiveness for injection from multirow holes", Jn. of Eng. For Power, Vol. 101, 1979, pp. 101.

Sheen, J.R., "Heat transfer enhancement within a turbine blade cooling passage using ribs and combinations of ribs with film cooling holes", Transactions of ASME, International Gas Turbine and AeroEngine Congress and Exposition, June 13-16,1994.

Simonich, J.C., and Moffat, R.J., "Liquid crystal visualization of surface heat transfer on a concavely curved turbulent boundary layer", Journal of Engineering for Gas Turbines and Power, July 1984, Vol. 106, pp. 619-627.

Simonich, J.C., and Moffat, R.J., "New technique for mapping heat transfer coefficient contours", American Institute of Physics, Rev. Sci. Instrum. 53(5), May 1982, pp.678-683.

Sparrow, E.M., et. al., "Turbulent Heat Transfer in the thermal entrance region of a pipe with uniform heat flux", Apple. Sci. Res. Section A, Vol. 7, pp. 37-52.

Thielbahr, W.H., "Heat transfer to highly accelerated turbulent boundary layer with and without mass addition", Trans. ASME, Jn. Of Heat transfer, Vol. 3, 1970.

Thielbahr, W.H., "The turbulent boundary layer on a porous plate: Experimental heat transfer with moderately strong acceleration", trans. ASME, Jn. Of Heat transfer, Vol. 94, 1972, pp.111.

Torii, K., "Heat transfer and skin friction in a turbulent boundary layer with mass addition", Proc. 3rd Int. Ht. Conf., AIChE/ASME, 1966.

Wagner, J.H., et.al., "Rotating heat transfer experiments with turbine airfoil internal flow passages", 1986, ASME Paper 86-GT-133.

Wang, Z., et. al., "A color image processing system for transient liquid crystal heat transfer experiments", Transactions of ASME, 94-GT-290.

Wang, Z., et. al., "An advanced method of processing liquid crystal video signals from transient heat transfer experiments", Transactions of ASME, 93-GT-282.

Woodmansee, W.E., "Aerospace thermal mapping applications of liquid crystals," Applied optics, Vol.7, No9, Sept. 1968, pp. 1721-1729.

Wu, C.S., and Louis, J.F., "A comparative study of the influence of different means of cooling on the performance of a combined (Gas and Steam) Cycle", Journal of Engineering for gas turbines and Power, vol. 106, 1984, pp. 750-755.

Zhang, L., and Han, J.C., "Influence of mainstream turbulence on heat transfer coefficients from a gas turbine blade", Journal of heat transfer, 1994, Vol. 116, pp. 896-902.

MICHIGAN STATE UNIV. LIBRARIES
31293017103866